Master of Science Thesis

Dosimetric Verification of Intensity Modulated Radiotherapy Treatment Plans with Radiographic Film

Sonny La

Supervisors: Tommy Knöös & Per Nilsson

Department of Medical Radiation Physics
The Jubileum Institute
Lund University, 2004

LUJI-RADFY-EX-3/2004

Ny strålbehandlingsteknik mot cancer

Idag behandlas cancer med bl.a. strålbehandling, tyvärr ger denna många gånger biverkningar. Detta beror på att strålningen inte bara skadar cancerceller utan även friska celler, eftersom strålningen måste passera frisk vävnad för att nå in till cancertumören. Det har nyligen utvecklats en ny strålbehandlingsteknik som kan minska strålningen till frisk vävnad samtidigt som tumören ges en hög stråldos. Tekniken går ut på att man med många små strålfält kan koncentrera *stråldosen*, dvs. den absorberade energin, bättre till tumören och således undvika för hög stråldos till frisk vävnad. Tekniken kallas IMRT som står för **I**ntensitets**m**odulerad **R**adio**t**erapi och är en komplicerad krävande teknik. Tekniken går ut på att man bestämmer önskad stråldos till tumören och högsta tillåtna stråldos till omkringliggande frisk vävnad. Ett datorprogram räknar utifrån dessa satta kriterier ut bästa fältsammansättningen, oftast bestående av tiotals till över hundra små strålfält.

IMRT är en teknik som kan medföra stora förbättringar om man lyckas koncentrera stråldosen till tumören. En liten felpositionering av patienten eller felberäkning av programmet kan dock medföra att stråldosen istället koncentreras till organen runt omkring tumören, dvs. friska organ som man vill undvika att bestråla. Efter att man räknat fram en plan för patientbehandling krävs därför en grundlig undersökning av stråldosfördelningen innan patienten behandlas. Svårigheten ligger i att man inte kan mäta direkt i patienten hur *dosfördelningen* ser ut, eller med andra ord, hur hög stråldosen är på olika områden i patienten. Istället flyttar man över behandlingsplanen för patienten (med exakt samma fältsammansättning och bestrålningstid) på ett fantom som är tillverkat av vävnadsekvivalent material som ska motsvara människokroppen. Detta fantom är tillverkat så att man kan stoppa in olika typer av detektorer, exempelvis strålkänslig film. Filmerna mäter dosfördelningen som sedan kan jämföras med den som är beräknad i datorprogrammet. Om dessa stämmer överens inom rimliga gränser väntar man sig att det även gör det inuti patienten. Då har man lyckats med sin behandlingsplan och patienten kan börja behandlas. Syftet med detta arbete har varit att finna ett pålitligt system för att verifiera IMRT-behandlingar, så att patienter kan börja behandlas med den nya tekniken vid universitetssjukhuset i Lund. I arbetet har huvudsakligen film använts och detta med lovande resultat som kan leda fram till ett tillförlitligt verifieringsystem (se Figur 1). Arbetet har även kompletterats med mätningar av andra detektorer som jonkammare och termoluminiscensdetektorer (TLD).

Figur 1. Figuren visar ett fantom innehållande två filmer som bestrålas med en linjär-accelerator.

TABLE OF CONTENTS

ABSTRACT

Intensity modulated radiation therapy (IMRT) is a fairly new modality in the treatment of cancer with radiotherapy. The original idea is Swedish and has existed for more than 20 years. But it is only in recent years that clinics have implemented the IMRT technique. IMRT uses many segments (small subfields) that build up radiation fields with nonuniform energy fluence. With this technique, better target conformity can be achieved and the absorbed dose to healthy tissues in the vicinity of the tumour can be limited. The purpose of this work is to find a reliable method to verify IMRT delivery, which can lead to commissioning of the IMRT technique at Lund University Hospital. The dosimetric equipment chosen to verify the IMRT delivery has been radiographic film, complemented with ion chamber measurements for absolute dose determination.

The verification has been performed on a phantom case, which is part of the QUASIMODO project used as an external audit of our dosimetric system. Additionally, a clinically patient case was also verified. Both treatment plans were optimized in the Oncentra Treatment Planning (OTP) system and forward calculated in Helax-TMS.

The EDR2 film from Kodak is a rather new type of radiographic film that has been used throughout this study. It was shown that the EDR2 film could accurately be used, within 2%, for relative as well as absolute dose measurements, down to a depth in the patient/phantom of at least 20 cm, when ignoring the build-up region. Absolute dose measurements with a cylindrical ion chamber (NE 2571 0.6 cm^3 Farmer type) showed, on the other hand, discrepancies up to 8% when compared to calculations by the treatment planning system (TPS). The reason for this might be due to partial irradiation of the ion chamber in IMRT. Thermoluminescent dosimeters (TLD) were used as an alternative detector for comparison and the result was within 2% of the TPS calculations.

With proper care the film dosimetry can be used to verify IMRT delivery. But before that, the large discrepancies with ion chamber measurements have to be further investigated. Many more cases have to be verified to get a better statistical base.

I. INTRODUCTION

Surgery, chemotherapy and radiation therapy (also called radiotherapy) are today the most common and important methods for treatment of cancer. Before the choice of treatment modality an extensive examination of the patient has to be performed to establish the tumour type, origin and the extension of the disease. Some tumours are, due to its size and general location classified as inoperable. Chemotherapy is sometimes problematic due to the patient's medical condition and is also not suitable for local treatment. In these situations radiation therapy might be the method of choice. Radiotherapy is also, however, many times combined with surgery and chemotherapy (SBU-rapport nr 129/1 1996 chap. 3).

Today it is well accepted that tumour control probability (TCP) and normal tissue complication probability (NTCP) have sigmoidal-shaped dose-response curves (see Figure 1). For normal tissue complications, radiation response also depends on the volume of tissue irradiated. Some tissues have a higher dose-volume dependency than others, e.g. kidney and lung are more dose-volume dependent than the spinal cord. The success of radiation therapy is therefore dependent of the radiosensitivity of the tumour being treated relative to the structure of the surrounding normal tissues. The goal in radiation therapy is to separate the TCP and NTCP curves as much as possible (Amols *et al.* 2003). In conventional radiation therapy the patient is treated with open fields with uniform energy fluence from each field. Wedged fields are used to get a better dose conformity around the target and hence a better separation of the TCP and NTCP curves. However, in some cases the absorbed dose to the organs at risk (OAR) can still be unacceptably high. This is where conventional radiation therapy isn't successful enough and a better treatment technique is needed.

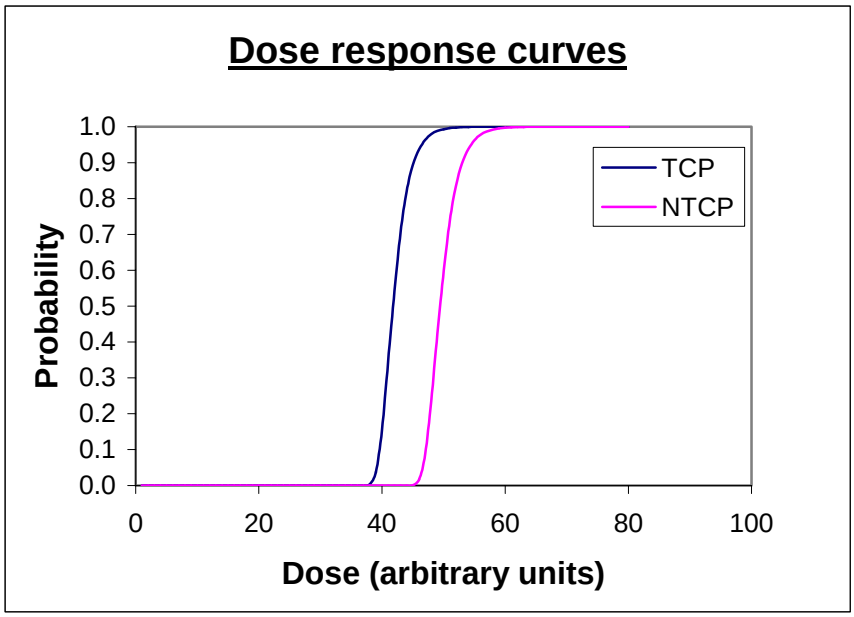

Figure 1. Schematic dose response curves for tumour and normal tissue. TCP and NTCP stand for tumour control probability and normal tissue control probability, respectively.

Intensity modulated radiation therapy (IMRT) is a relatively new modality in radiation therapy. The theory of IMRT was first proposed in 1982 (Brahme *et al.* 1982). The main advantage of IMRT contra conventional radiation therapy is that IMRT can better conform the absorbed dose around the tumour (or target) and thus

limit the absorbed dose to the OAR (see Figure 2). The concept of IMRT is to use nonuniform energy fluence from each field to achieve better conformity around the target. IMRT uses several beams from different directions, usually equally spaced around the patient. One possible negative aspect of IMRT is that the radiation will be delivered from a wider range of directions. This will lead to that low dose regions will be spread over a larger volume of the patient. Low dose regions could give rise to complications for the patient, but no clinical studies have given information about this yet (Bäck 2003).

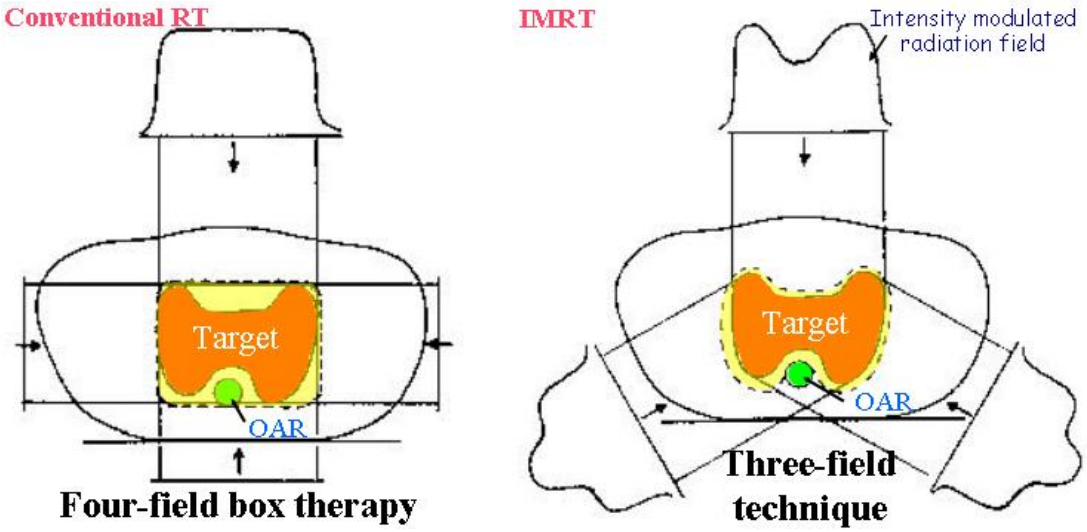

a) **b)**

Figure 2. Comparison of the dose conformity around the target between conventional radiation therapy (RT) and IMRT. a) A four-field box technique with conventional radiation therapy. b) A three-field technique with IMRT showing the nonuniform energy fluence from each field. (Adopted from Brahme, Radiotherapy & Oncology (1988) 12:129-140.)

Figure 3. The multi leaf collimator (MLC) leaves that can form irregular shapes which can better match the target. (From Elekta Oncology Systems.)

There exist several types of techniques to deliver the desired IMRT plan. One technique is by fabrication of custom-designed three-dimensional (3D) physical compensators that can be inserted between the patient and the radiation source. These compensators will be unique for each beam and treatment plan. This technique is very tedious but do not require any major investments in technology, e.g. accelerators with multi-leaf collimators (MLC). The way to deliver the dose is also very similar to conventional radiotherapy. However, a more common way to deliver the IMRT plan is by using a computer controlled MLC (see Figure 3) to shape each segment within an IMRT beam. The MLC-based IMRT delivery is usually divided into two categories: 1) dynamic MLC (dMLC) or sliding window technique and 2) segmented MLC (sMLC) or step-and-shoot technique. In dMLC, the MLC leaves are continuously moving while the radiation is on, whilst sMLC utilizes a sequence of multiple, smaller fixed subfields. When the dose from the first segment has been delivered the radiation is terminated and the MLC leaves will move to the next segment and the radiation starts again. This procedure will continue until the last segment has been given, thereof the name step-and-shoot (Carlson D. 2001, Chui C-S. *et al.* 2001). In this study, we will only concentrate on the verification of IMRT delivery with the sMLC approach. A simplified example of a sMLC is shown in Figure 4 to illustrate the technique. The treatment is built up with three beams, each beam consisting of three segments resulting in a total of nine segments.

Segmented MLC IMRT has gained popularity due to its simplicity. There are, however, both positive and negative aspects with this technique. The advantages of this method are that it is similar to conventional radiotherapy and it is easy to understand. There is no need to control the MLC leaf speed and an interrupted treatment is easy to resume. It requires fewer monitor units (MUs) per given dose compared to dMLC. The main disadvantage of this technique is the prolonged treatment time and dosimetric errors that may be introduced during discretization of a continuous intensity profile. In dMLC the treatment time is shorter. The intensity pattern is decomposed into a sequence of segments with very fine small steps between the segments. The MLC control system is more complex and the control of the MLC leaf speed is crucial. Normally it requires more MUs to deliver a given dose than with sMLC. To mention an example, Memorial Sloan-Kettering Cancer Center in NY found that they required 20% more MUs with dMLC than with sMLC. In contrast to this, the total delivery time with dMLC was just half of the sMLC delivery time (Chui C-S. *et al.* 2001). A larger number of MUs delivered gives more importance to MLC parameters such as intraleaf transmission (through the leaf) and interleaf transmission (between the leaves) (Xia *et al.* 2001, Carlson 2001). The use of more MUs during dMLC will also lead to possibly more scattered or transmitted radiation that in turn can reach other parts of the patient and contribute to unwanted absorbed dose.

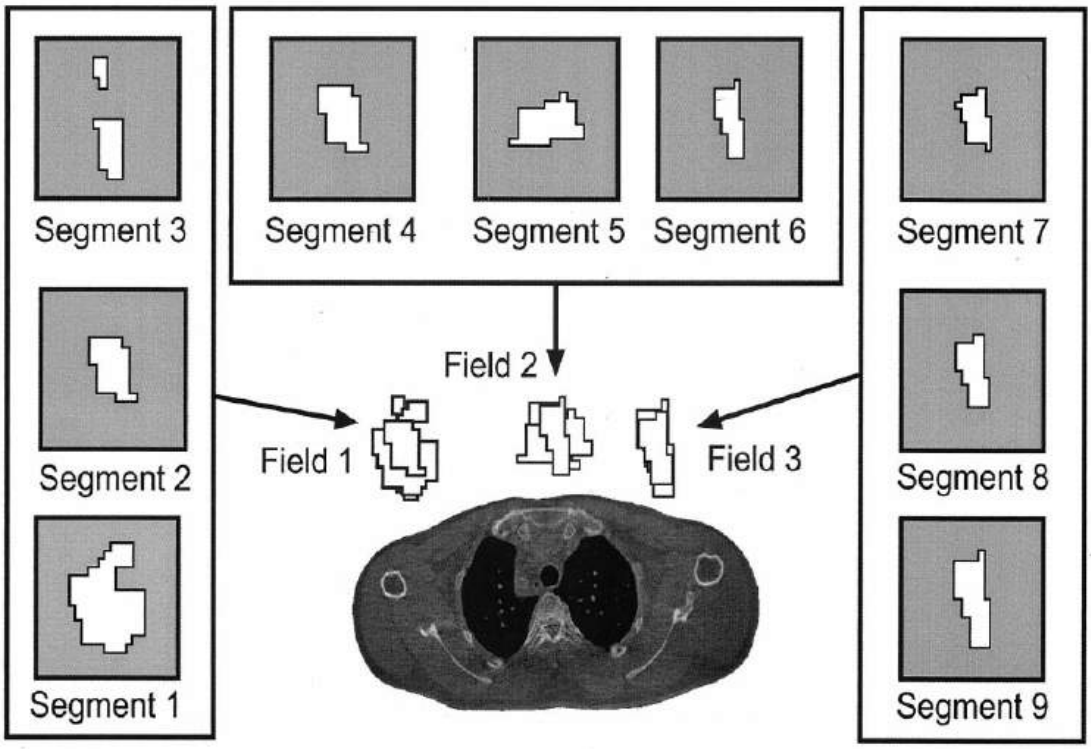

Figure 4. An example of how IMRT fields are built up of several segments. This is just a simplified overview of an IMRT treatment consisting of three fields with altogether 9 segments. Normal IMRT plans consist of many more segments. (From Carlson 2001.)

IMRT treatment planning process

The treatment planning process of IMRT is similar to conventional radiation therapy with a few differences (see Figure 5). After the patient gets the diagnosis and radiation therapy has been chosen as the treatment modality, the patient will go to the simulator. Some kind of custom designed fixation mould will be made to immobilize the patient in the treatment position. Thereafter the patient will be CT scanned in this position, with the fixation device, for image acquisition. These images will be used by the oncologist for delineation of structures such as the target and the OARs. When the delineation is completed, the optimization of the dose plan will begin. IMRT treatment planning is usually performed using an inverse treatment planning (ITP) algorithm as opposed to forward planning in conventional radiation therapy planning. In forward planning the dosimetrist chooses the energy, the number of beams, the beam directions, the shapes of the beams, the beam weights and the beam modifiers. In ITP the treatment planner still have to choose the energy, the number of beams and usually also the beam directions but not the beam weights and the beam modifiers. Additionally, the user has to specify dose volume constraints for the target and the OARs which will form the objective function. A computer program will then calculate/optimize the intensity modulation that best meets these constraints. The MLC settings that can deliver the intensity modulation are also calculated. This latter process is usually named segmentation. After segmentation the resulting dose distribution is recalculated and the objective function is evaluated. The optimization and the segmentation are performed within a loop that is repeated until no further improvement can be achieved.

In summary one can see it as follows: the user specifies the desired dose distribution and the computer will do the rest to meet the user-specified criteria. A

condition is that the planner sets some realistic dose constraints. These are not always achieved, thus the whole process continues in a loop where the planner together with the physician and the physicist has to change the constraints until what is considered a clinically acceptable plan. When the treatment plan has been accepted, the planning data is transferred to the linear accelerator and the patient treatment will proceed from there.

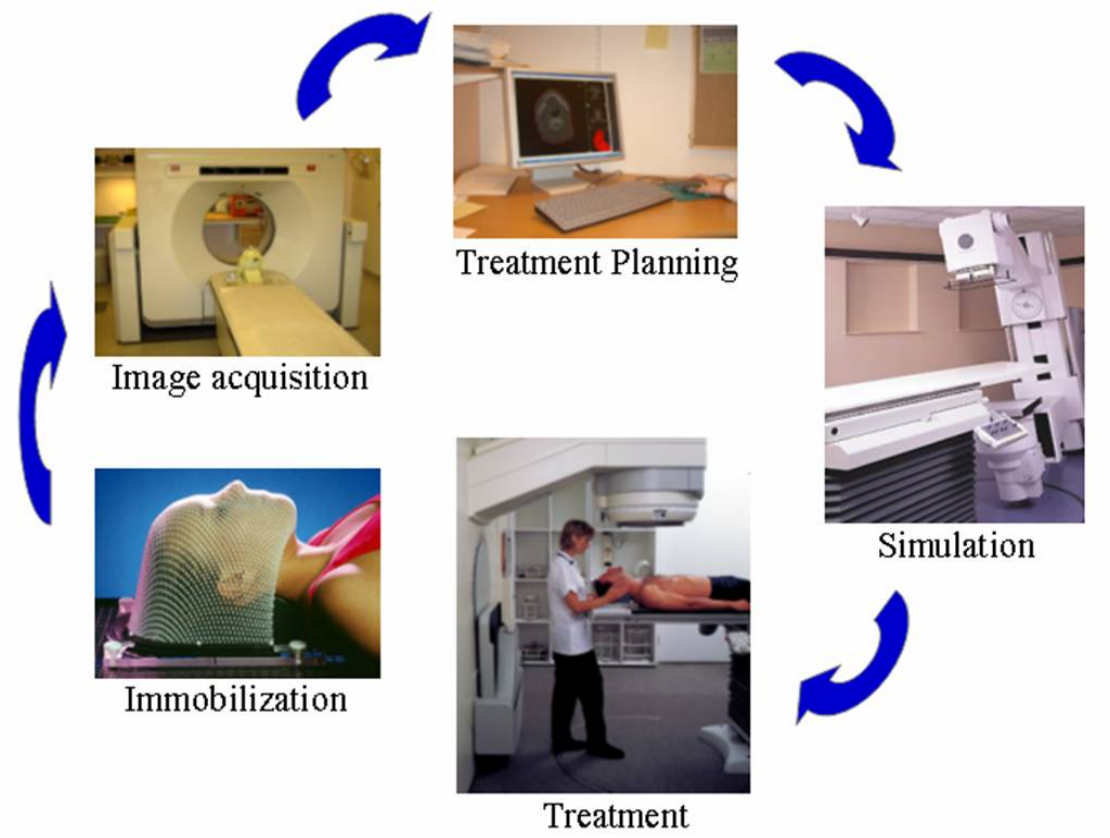

Figure 5. The overall process of IMRT planning and delivery, from immobilization to treatment.

Before the treatment can start, dosimetric and quality control (QC) tests must be performed to verify that the equipment functions properly, and that the dose prescription and the treatment plan can be accurately delivered to the patient. In conventional radiation therapy it is common to have two independent MU calculations for patient treatment. Calculation of the number of MUs can usually be carried out manually in conventional therapy. The absorbed dose at a certain position is dependent on the beam energy, the field size, the treatment distance and the depth. In IMRT the shapes of the segments are very complex and the number of the segments can be high, thus it is not practical to make manual calculations in the manner described above (LoSasso *et al.* 2001). This will result in that other approaches have to be applied to verify that the calculated and the delivered dose are in close agreement. One pre-treatment check can be carried out by measuring point doses in a phantom with an ion chamber and compare the result with prescribed doses. To do this the treatment plan of the patient must first be transferred to a phantom and be recalculated in the treatment planning system (TPS) (LoSasso *et al.* 2001). In IMRT there are sharp dose gradients and a small displacement of the ion chamber can result in significant errors. To get an overview of the dose distribution, a planar detector e.g. film is preferred. If the measured absorbed dose distribution agrees with the calculated

absorbed dose distribution within the phantom, it is assumed that it will be the case in the patient too.

This study has concentrated on this step in the process – the verification of the delivered dose distribution for IMRT treatments. The planar detector of choice is radiographic film, but additionally point measurements with ion chambers have also been performed. The main purpose of this study is to:

Find a way to verify IMRT delivery with film, which can lead to commissioning of IMRT for patient treatments at Lund University Hospital.

IMRT verification

When an IMRT treatment plan has been accepted for patient treatment it has to be verified, according to the description above. The method adopted here is to transfer the CT based treatment plan to a homogenous phantom. The plan is then recalculated in the TPS for this phantom. Measurements can then be performed in the phantom either with film or point detectors like ion chambers. The calculated dose distribution in the phantom is compared with measurements in the phantom (see Figure 6). The phantoms are usually geometrically regularly shaped, rectangular, cylindrical or a combination of both. When calculating the dose distributions in the phantom, exactly the same beam and MLC settings are used as in the patient case. If the measurements and the calculations in the phantom are within acceptable tolerances, the IMRT plan is considered to be accurate to deliver to the patient. Relative 2D dose distributions are commonly measured with film. But film can also be used for absolute dose measurement if there is a trustworthy film dosimetry system. For absolute point dose measurements, ion chamber and thermoluminescent dosimeters (TLD) could also be used.

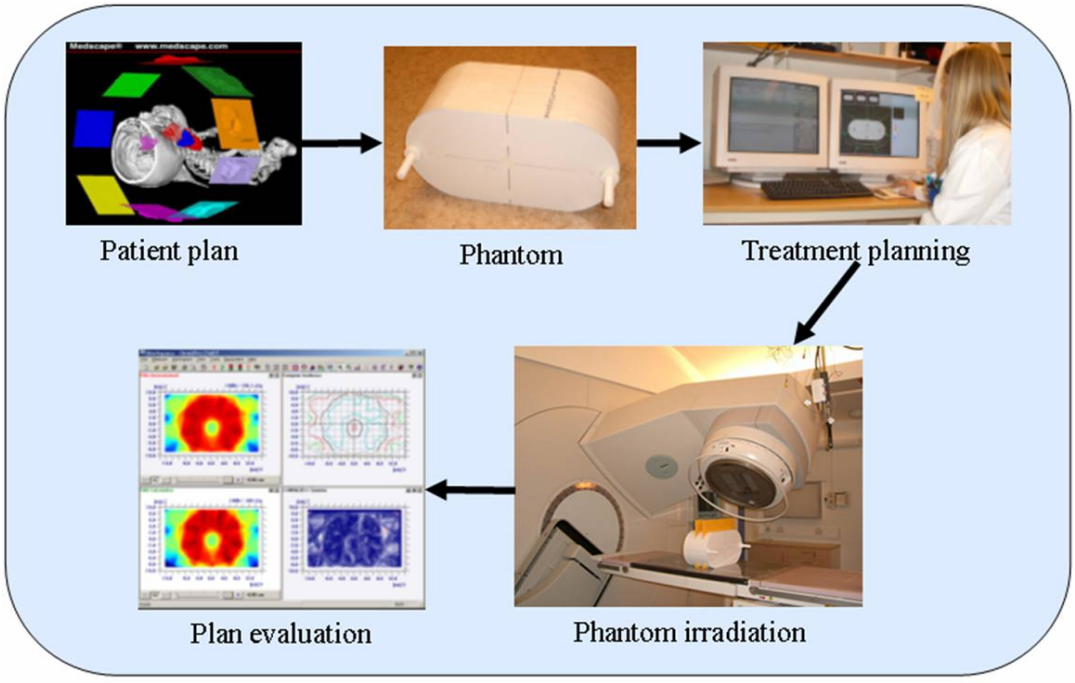

Figure 6. The verification process of IMRT treatment plans before patient treatment. The patient treatment plan is transferred to a phantom, with the same MLC and MU settings. Thereafter dose distributions in the phantom are recalculated and measurements in the phantom are performed with e.g. film. The results from the films are compared with TPS calculations.

II. MATERIALS AND METHODS

Dose delivery

All irradiations in this study were performed on an Elekta SL*i* linear accelerator (Elekta, Crawley, West Sussex, U.K.) supplied with photon beam qualities 6 MV and 10 MV x-rays (see Figure 7). The accelerator consists of 40 leaf pairs all with a projected leaf width of 10 mm at isocentre level and with a thickness of 70 mm. The dose rate in isocentre was 320 MU/min and 370 MU/min for 6 MV and 10 MV photon beam energy, respectively. The step-and-shoot technique was used to deliver the prescribed IMRT dose plan. The control system of the accelerator was equipped with the software version (Desktop Pro Release 5.0) from Elekta allowing for so called grouped treatments where several segments even with different gantry angles can be delivered with a single initiation (the so called one-button treatment technique). This will result in shorter treatment times due to no human interference being required between segments.

Figure 7. The Elekta SL*i* linear accelerator used in this study.

Treatment planning system

The treatment planning system used to optimize the IMRT plans with inverse treatment planning was the Oncentra Treatment Planning (OTP) system, ver. 1.2 (Nucletron, Veenendaal, the Netherlands). The radiation therapy plans were then transferred to and subsequently recalculated in our clinical treatment planning system Helax-TMS ver. 6.1A SP 1 (Nucletron, Veenendaal, the Netherlands). This TPS was used to determine the correct number of monitor units (MUs) for each segment as well as to transfer the plan via DICOM-RT to the record-and-verify system (Oncentra-Visir, Nucletron). The Helax-TMS system has been in clinical use for many years at the department and its performance has been verified in a number of scientific publications (see e.g. Knöös *et al.* 1994). OTP is not yet in clinical use and therefore the final calculations were performed in Helax-TMS.

Film dosimetry

Radiographic film is commonly employed as a dosimeter for validation and QA test of IMRT fields, due to its high spatial resolution. In the first half of 2001, a new ready-pack film with enhanced dynamic range called EDR2 was released (Extended Dose Range 2, from Eastman Kodak Co., Rochester, NY, see Figure 8). There are some improvements in the EDR2 film compared to earlier radiographic films used for dosimetric purposes. Compared to e.g. Kodak XV2 film, the grain size in EDR2 film is about one tenth smaller and more uniform in shape. The silver content is also much lower in EDR2 films, significantly lowering the sensitivity of the film. The film can therefore be exposed to much higher doses before it becomes saturated which makes it suitable for IMRT verification. The smaller grain size together with the reduced silver content might also reduce the energy dependence (Olch 2002).

EDR2 films of size 25.4x30.5 cm^2 were used throughout this study. To avoid any potentially interbatch differences all films during a single experiment were taken from the same batch. The film envelopes were punched in the corners in order to remove any air pockets. A Dürr film processor (Dürr – Dental D-7120 Bietigheim, Germany) at the Radiation Therapy department was used to develop all films. All films exposed during one session were processed and developed at the same time together with a set of calibration films. An unexposed film was at the same time developed to determine the optical density (OD) for the corresponding base and fog. With this technique, any eventual variations in the processing conditions were minimized. A 12-bit film digitizer (VXR-12, Vidar Systems Corporation, Herndon, VA, see Figure 9) was used to scan all films with a resolution of 75 dpi and the OmniPro-Accept 6.1 respectively OmniPro I'mRT software (both from Scanditronix/Wellhöfer, Uppsala, SWEDEN) were used to analyze the scanned films.

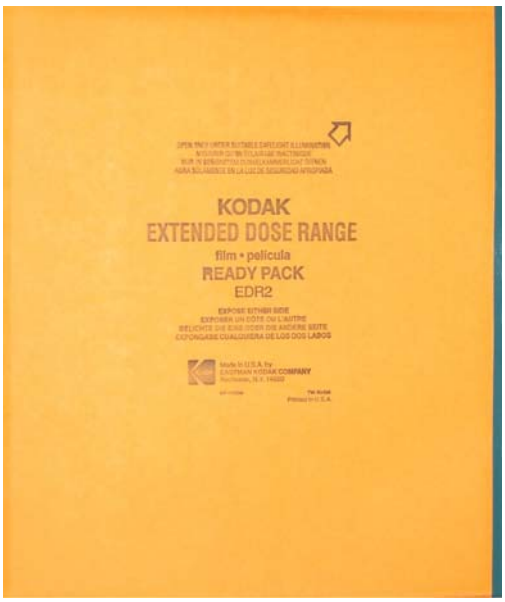

Figure 8. The EDR2 film enclosed in its ready pack envelope. All film measurements in this study were performed with the EDR2 film of size 25.4x30.5 cm^2.

Figure 9. The Vidar scanner used to digitize the film measurements.

Film calibration

Before calibrating the film, we have to calibrate the scanner by converting the analogue to digital converter (ADC) values to OD. This is done via a film strip supplied from Kodak with varying known OD values.

Sensitometric curve for EDR2 film

A sensitometric curve describes the relationship between the optical density of the film and the absorbed dose delivered to the film. Calibration films were irradiated with 6 MV and 10 MV photons beam energies for sensitometric curve determination. The films were placed perpendicular to the central beam axis under 5 cm of polystyrene with 10 cm of polystyrene underneath the film. The gantry angle was 0°, the collimator angle 90° and the source-to-surface distance (SSD) was 100 cm. Eight different dose levels (0.25, 0.5, 1.0, 1.5, 2.0, 2.5, 3.0, and 3.5 Gy) were delivered with a field size of 5x5 cm^2 with one field per film resulting in eight sheets of film plus an unexposed film for determination of the OD corresponding to the base and fog in such a calibration set. The MUs required to deliver the doses were calculated from physical data protocols used in the clinic. However, the protocols are based on measurements in water and not in polystyrene. Relative dose measurements in water and polystyrene differ by only 1.1% (Cadman *et al.* 2002). So there is no need to correct the absorbed dose in polystyrene. The absorbed doses were corrected for any output variations of the accelerator to obtain exact doses delivered to and absorbed by the films. This correction was obtained by output measurements before and after each experiment, and the average value from these two measurements were taken to correct the absorbed doses delivered from the machine. Exposing eight films per calibration occasion is both time consuming and expensive, and therefore it is of value if all eight fields could be delivered to one single film (see Figure 10). We tested therefore if an eight-field film could reliably replace “the eight single fields” calibration technique. A corresponding relationship between the ODs on the eight-field film and the ODs on the single-field exposed films could be established after a couple of experiments performed at different occasions.

All films exposed at one occasion were processed at the same time to avoid any day-to-day variation of the film processor. The ODs were read using a manual densitometer (Macbeth, model TD932, Newburgh NY, see Figure 11). The densitometer can be used in roomlight conditions. The background of each film was subtracted using the reading from the unexposed film and a sensitometric curve could thus be obtained between the ODs and the absorbed doses delivered to the films.

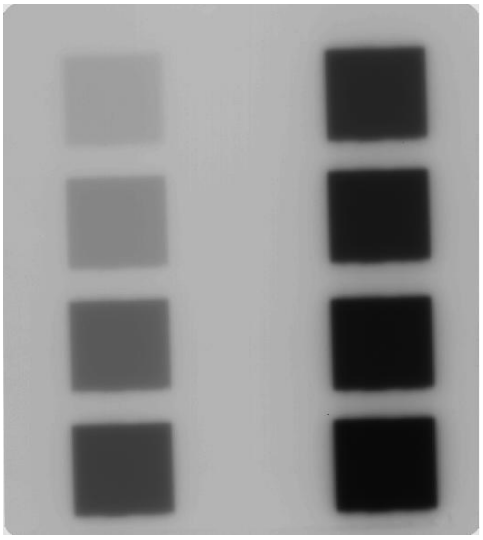

Figure 10. A single calibration film exposed to eight dose levels for determination of the sensitometric curve. Such a film is taken at each test occasion to minimize day-to-day variations. The dose levels are 0.25, 0.5, 1.0, 1.5, 2.0, 2.5, 3.0, and 3.5 Gy, beginning from the left column and going downwards.

Figure 11. The Macbeth densitometer TD932 used in our clinic. The densitometer is used to measure the OD at a particular location on a film.

Validation of film dosimetry for other irradiation conditions

Prior to using the film dosimetry system for IMRT exposure tests, validation of the relationship between OD and absorbed dose delivered in simple geometries has to be performed. The first step is to move away from the calibration geometry with small perpendicular fields impinging on the film. Films were therefore exposed to different field sizes and at various phantom depths. Also the influence of different film orientations in relation to the radiation beam axis was tested. The films were scanned in the Vidar scanner and ODs were converted to absorbed dose according to the sensitometric curve obtained at each session (see previous section).

- **Single quadratic beams, film oriented normal to the radiation beam axis**
  Films were placed at five different depths (1.5, 5, 10, 15, 20 cm) in a 30x30x30 cm^3 slab phantom of polystyrene. The films were oriented perpendicular to the beam axis and irradiated with 250 MU (approximately 3 Gy at dose maximum). The SSD was 90 cm and three field sizes were used (5x5 cm^2, 10x10 cm^2, 20x20 cm^2).

  The measured absolute dose distributions were compared with TPS calculated data using the exported dose matrix from Helax-TMS. The analysis was performed with commercial software (OmniPro I'mRT from Wellhöfer Scanditronix, Uppsala, Sweden)

- **Single quadratic beams, film oriented parallel to the radiation beam axis**
  In order to determine the performance of the film oriented parallel to the beam direction, a depth dose curve was determined with film (see Figure 12). The same polystyrene phantom as above was used but the slabs were oriented parallel to the beam axis. A film with its longer side was placed between two slabs in the crossplane direction, and the whole phantom was held tightly together with four screw clamps. The edge of the film was positioned just

above the edge of the phantom. The film was then punched with a needle along the edge of the phantom for alignment purpose. The reason to not placing the film with its shorter side upwards was to minimize the extra attenuation that the film and the envelope may cause. The film was positioned 0.5 cm off-axis in the inplane direction to avoid coincidence with the central beam axis, which could otherwise cause some increased attenuation. The gantry angle used was 0°, collimator angle 90°, SSD 90 cm and the field size was 10x10 cm^2. The measured depth dose profile with film was obtained applying the sensitometric curve and the result was compared with a measured depth dose curve in water and with a TPS calculated depth dose curve in polystyrene exported from Helax-TMS.

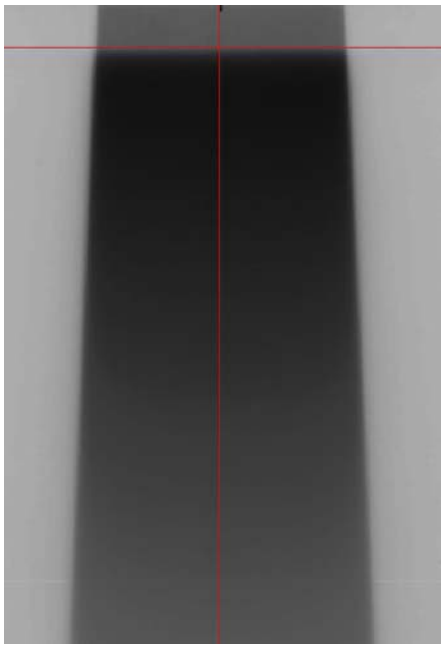

Figure 12. An exposed film for depth dose determination. The film was placed 0.5 cm off-axis to avoid coincidence with the central beam axis and thus minimizing attenuation disturbances caused by the film. The top red line indicates the entrance surface of the phantom and the vertical line the position of the extracted depth dose.

- **Multiple quadratic beams, film oriented parallel to the radiation beam axis**

  A two-field and a four-field opposing field treatment plan were created in the TPS with 10x10 cm^2 fields on a polystyrene phantom called CarPet. This phantom was constructed by an international group of physicists participating in the QUASIMODO[1] project which is part of the EU sponsored project ESQUIRE[2] run by ESTRO[3]. The phantom consists of 16 slices of polystyrene,

[1] QUASIMODO (Quality Assurance for Intensity Modulated Radiation Oncology)
[2] ESQUIRE (Education, Science and QUality Assurance for Radiotherapy)
[3] ESTRO (European Society of Therapeutic Radiology and Oncology)

each 1 cm thick (see Figure 13). Measured absorbed dose distributions with the film were compared with the TPS generated treatment plans.

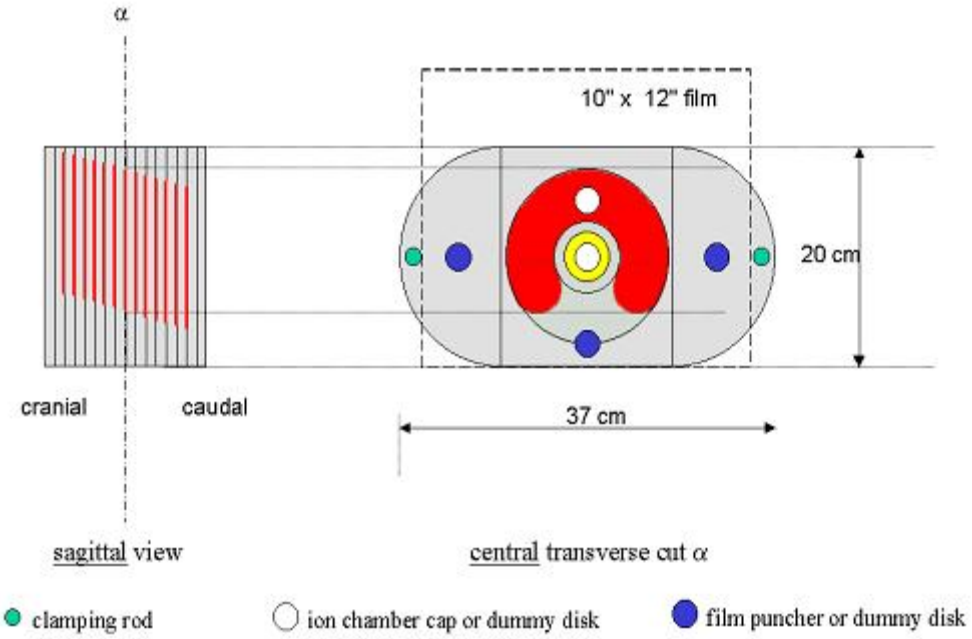

Figure 13. A schematic view of the CarPet phantom in sagittal and axial view. (Courtesy of QUASIMODO.)

- **IMRT beams**

An IMRT plan which is part of the QUASIMODO project was used as an external audit of our dosimetric system. This plan was optimized and segmented in the OTP system and recalculated in Helax-TMS. Nine beams were used to optimize the plan resulting in altogether 120 segments. The prescribed doses were 1.8 Gy to the target and 1.0 Gy to the OAR, respectively. The treatment plan was applied to the CarPet phantom with the isocentre positioned in the geometric centre of the phantom, which is the same as the centre of the OAR. Four films were placed at ±1 cm and ±4 cm off-axis. The films were scanned and evaluated.

The same plan, with all gantry angles changed to vertical, was also applied to the 30x30x30 cm^3 polystyrene phantom and verified, field by field, with films normal to the central beam axis. Each film was placed at 5 cm depth.

The TPS does not have the option of transferring a calculated patient plan to a phantom and still keep the calculated MU settings when the plan is broken down to field specific sub-plans. When a plan is transferred to a phantom, a recalculation has to be executed. To best match the same number of MUs per field, 0.1 Gy to the isocentre in the 30x30x30 cm^3 polystyrene phantom was prescribed.

A second verification was performed with a clinical patient case except for the field by field verification. The patient was a 61 year old male, with the diagnosis squamous cell carcinoma of the tonsil with lymph node metastases. Seven beams with altogether 52 segments were used to optimize the plan (Ambolt, 2004). Two films were taken at +1 cm and -4 cm off-axis (see Figure 14). The absorbed dose was also determined with an ion chamber at the isocentre, corresponding to the geometric centre of the CarPet phantom.

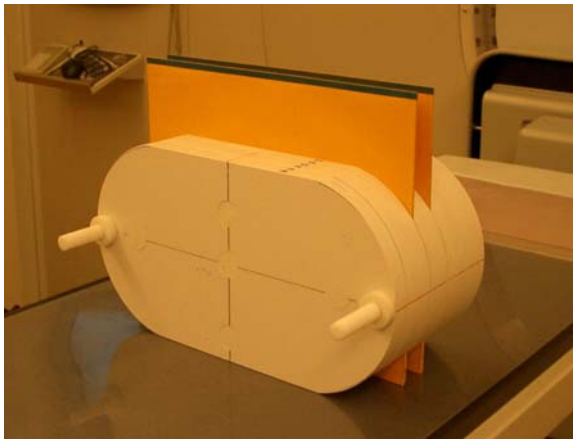

Figure 14. The CarPet phantom loaded with film for the patient plan exposure.

Dose measurement with ion chamber

The verification of IMRT-plans was complemented with ion chamber measurements in the CarPet phantom (see Figure 15). This is accomplished by removing the dummy discs (see Figure 13). The absolute doses were measured in the OAR and in the target and compared with the film measurement and the TPS calculations. The clinical patient case was only measured in the isocentre corresponding to the position of the target in the patient. The ion chamber used was a cylindrical Farmer model (NE 2571 0.6 cm^3 Farmer chamber, see Figure 16). The measured absorbed dose was determined by first irradiating the phantom with an open 10x10 cm^2 field giving 1.0 Gy to the isocentre (equal to the ion chamber position), calculated from physical data protocols, and recording the charge collected. The measured charge with the ion chamber in the target and in the OAR, respectively, when the phantom was irradiated according to the treatment plan were then divided by this charge. Since this is performed during a rather short time period, neither corrections for accelerator output nor any changes in ambient conditions have to be applied.

Figure 15. The CarPet phantom with an ion chamber inserted and ready for exposure.

Figure 16. The Farmer type ion chamber (0.6 cm^3 NE 2571) with its corresponding build-up cap used for absolute dose measurement in the CarPet phantom.

Dose measurement with TLD

In addition to the ion chamber measurement, thermoluminiscent dosimeters (TLDs) were used to measure the absolute dose. This was accomplished in a similar manner as with the ion chamber measurements. A custom designed insert was inserted when removing the dummy discs. The irradiation was performed in the same manner as with the ion chamber measurements.

Dose comparison tool, Gamma evaluation method

When comparing two absorbed dose distributions, e.g. one measured and one calculated, the easiest way to do this is by comparing either the position of the isodoses or the absorbed dose differences at each position. However, this may not always be appropriate and misjudgements may occur. For example, in high-gradient regions the difference between two absorbed dose distributions can be very large, even though the isodoses are rather close to each other. On the other hand, the distance-to-agreement (DTA) method (Harms *et al.* 1998) between two isodose distributions can be large in regions with a very homogenous absorbed dose distribution, even if the absorbed dose difference may be small. The DTA is the distance between a measured data point and the nearest point in the calculated absorbed dose distribution that exhibits the same absorbed dose. In an IMRT plan there are regions with fairly homogeneous absorbed dose distribution as well as areas with high dose gradients. Evaluating the plan with either the dose difference or the DTA will yield poor results in certain areas. One way to overcome this problem is to study the dose difference in regions with a fairly flat dose distribution and to focus on the DTA in high-gradient regions. However, this can be a cumbersome procedure and a simpler way to estimate the goodness of agreement between two dose distributions is by using the so called gamma (γ) method. This method combines the two methods mentioned above, i.e. dose difference and DTA. The gamma method is used to quantitatively evaluate the agreement between two dose distributions. The user defines the dose difference and DTA pass-fail criteria. If both parameters are outside the pass-fail criteria the agreement fails according to the gamma method. The OmniPro I'mRT program has the gamma feature and is used to calculate all gamma values in this study.

The γ-value can be seen as a quality index. If

r_m is the measurement point,
r_c the spatial location of the calculated distribution relative to the measured point,
Δd_M the DTA criterion,
ΔD_M the dose difference criterion,
$D_c(r_c)$ the calculated dose in r_c, and
$D_m(r_m)$ the measured dose in r_m

the γ-value for a measurement point r_m is defined as:

$$\gamma(r_m) = \min\{\Gamma(r_m, r_c)\}\forall\{r_c\} \tag{1}$$

where

$$\Gamma(r_m, r_c) = \sqrt{\frac{r^2(r_m, r_c)}{\Delta d_m^2} + \frac{\delta^2(r_m, r_c)}{\Delta D_m^2}} \tag{2}$$

$$r(r_m, r_c) = \left| r_c - r_m \right| \tag{3}$$

and

$$\delta(r_m, r_c) = D_c(r_c) - D_m(r_m) \tag{4}$$

is the difference between the calculated and measured absorbed dose values. The pass-fail criteria therefore become

$$\gamma(r_m) \le 1, \quad \text{calculation passes,} \tag{5}$$

$$\gamma(r_m) > 1, \quad \text{calculation fails.} \tag{6}$$

The gamma calculation is then performed for all r_m. The reader is recommended to study Low *et al.* 1998 for a more fundamental description of the gamma evaluation method. An alternative way to calculate the index has been presented by Bakai *et al.* 2003.

III. RESULTS AND DISCUSSION

Film calibration

Table 1 summarizes the measurements of the ODs from the single-field exposed films and the 8-field film technique. For the 6 MV photon beam energy case, the average result is based on measurements at three separate occasions while for the 10 MV photon beam energy the results are from two measurements. Listed are also the standard deviations for the 6 MV case.

	----------6 MV----------				----------10 MV--------	
	8-field		**Single-field**		**8-field**	**Single-field**
Dose (Gy)	Net OD	SD	Net OD	SD	Net OD	Net OD
0.25	0.090	0.000	0.080	0.000	0.090	0.080
0.50	0.193	0.006	0.170	0.000	0.190	0.170
1.00	0.413	0.006	0.387	0.006	0.410	0.390
1.50	0.653	0.006	0.633	0.006	0.655	0.640
2.00	0.917	0.006	0.890	0.000	0.950	0.920
2.50	1.227	0.012	1.180	0.000	1.265	1.220
3.00	1.533	0.015	1.480	0.000	1.595	1.550
3.50	1.827	0.015	1.777	0.006	1.895	1.865

Table 1. The average result of the ODs on the 8-field film and the single exposed films for 6 MV and 10 MV photon beam energies. Three measurements were performed on three different occasions for the 6 MV photon beam energy case and also listed is the standard deviation (SD) of these three measurements. The results for the 10 MV photon beam energy case is based on two measurements.

Figure 17 shows the net OD for the single exposed films vs. the OD for the 8-field film for the two photon beam qualities 6 MV and 10 MV. The background from an unexposed film developed together with the calibration films was subtracted from the ODs of the films to obtain the net OD. The output from the accelerator was found to be very stable between the different sessions. Output variations less than 0.5% was recorded, and the ODs between the different sessions showed very similar results, which is shown in the small standard deviations in Table 1. This suggests that as long as we expose the 8-field film with the same dose levels and beam positions the distribution of scattered radiation from other fields will be constant over the entire film. This implies that only one eight-field film needs to be exposed for calibration purposes at each occasion. This procedure will save time, workload and films. The readings of the ODs of the 8-field film are converted to readings as if the film was single exposed by using the relationship that can be seen on the upper left corner in Figure 17. There seems to be only a small difference between ODs for the single exposed films versus the 8-field films when comparing 6 MV and 10 MV photon beam qualities (see Figure 17).

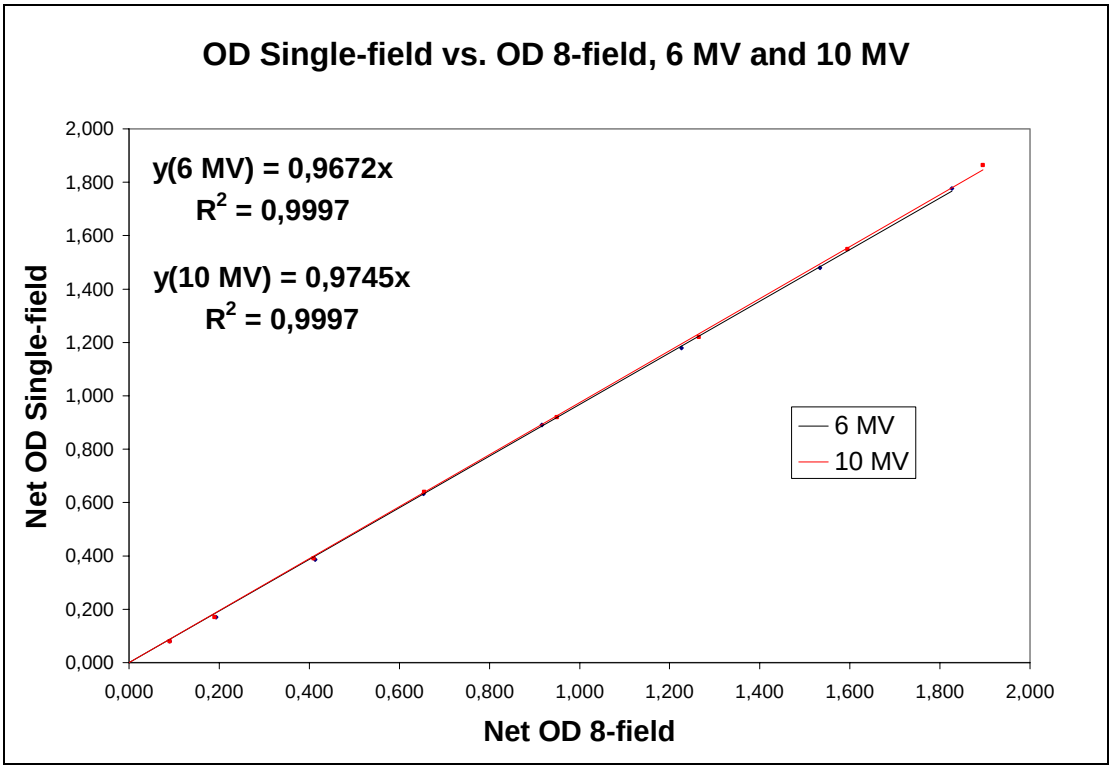

Figure 17. The relationship between ODs for single exposed films and 8-field films for the two photon beam qualities 6 MV and 10 MV. Linear regression lines are plotted in the graph together with the equations for these lines and corresponding R^2-values.

The sensitometric curves for EDR2 films in terms of OD vs. absorbed dose for the two photon energies 6 MV and 10 MV can now be obtained from the known doses delivered from the accelerator and from the measured ODs from a single calibration film. Figure 18 shows an example for the two energies studied. The relationship is rather close to linear over the entire range plotted. We have, however, fitted the sensitometric curves with a fourth order polynomial with R^2 values equal to unity. In our case the OD vs. absorbed dose up to about 3.5 Gy is plotted and there is still no tendency of film saturation. According to Esthappan *et al.* 2002 the EDR2 film does not saturate until about 7 Gy.

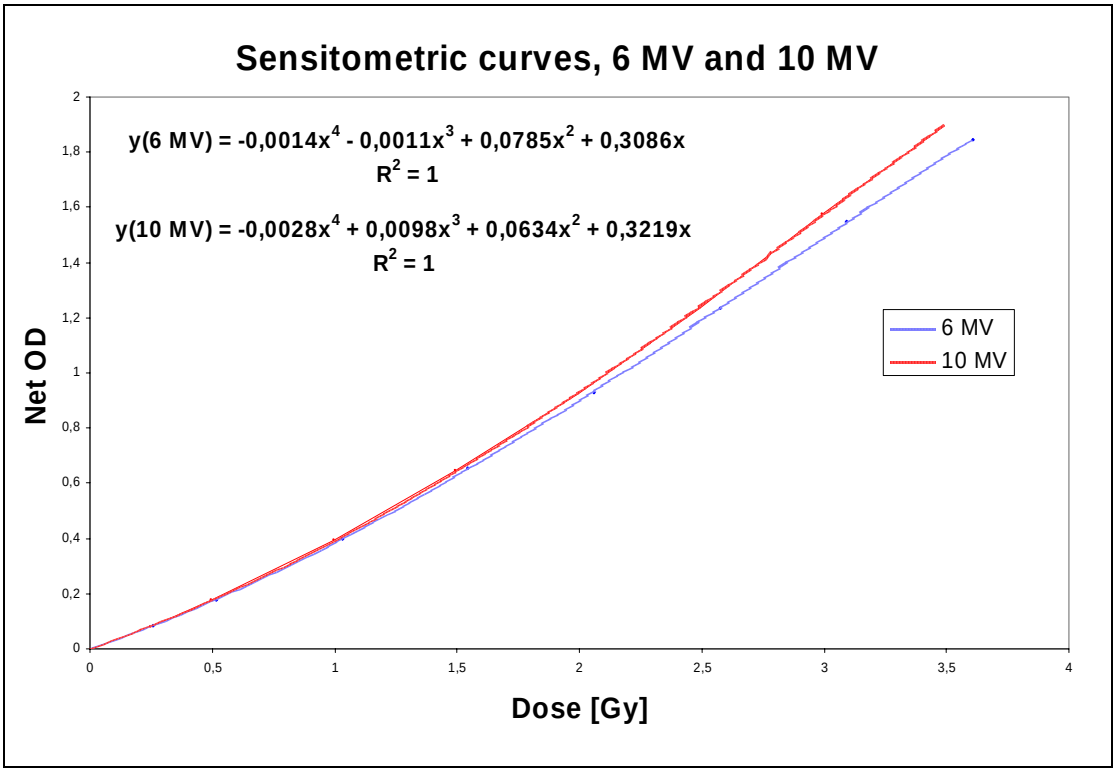

Figure 18. The sensitometric curves for the two photon energies 6 MV and 10 MV and their corresponding polynomial equations. It can be noted that the curves start to separate at higher doses.

As shown in Figure 18 the EDR2 film seems to have a minor energy dependence requiring individual sensitometric curves for the two photon beam qualities. The typical radiation therapy fraction dose is around 2 Gy where the curves start to diverge. Zhu *et al.* 2002 found that 6 and 23 MV photon beams have very similar sensitometric curves in contradiction to our result for 6 and 10 MV photon beams. Thus, for each beam quality we used a separate calibration.

Film dosimetry, like any other kind of dosimetry, requires that the dosimeter is stable in time and has a continued accuracy in its reading. Therefore a sensitometric curve taken at each test session or patient QA would be the ideal case. This would minimize the potential errors that the film may harbour from day to day tests. An additional advantage by calibrating the film at each exposure session is that one does not have to worry about output variations and different processor conditions from day to day.

Validation of film dosimetry for other irradiation conditions

The absolute doses evaluated from the film measurement (average from several point measurements at the centre of the field) with the film perpendicular to the beam direction for five different depths are listed in Table 2 together with calculated doses by the TPS. The percentage difference between the two is also listed as calculated from $(D_{meas.}-D_{calc.})/D_{calc.}x100$, where $D_{calc.}$ is the dose calculated by the TPS and $D_{meas.}$ is the absorbed dose measured with the film.

It has been shown that radiographic film exposed to field sizes smaller than 10x10 cm^2 and at depths less than 10 cm show little difference in their sensitivity (Zhu *et al.* 2002) which is in accordance with our results. At larger field sizes and at greater depths, however, the difference between calculated and measured absorbed doses can be quite large. This indicates that the sensitivity of the film varies with the beam

quality. This should not be a significant problem in IMRT since the field sizes are most often small for this treatment technique.

5x5 cm^2 field			
Depth (cm)	**Film dose (Gy)**	**TPS dose (Gy)**	**Diff. from TPS (%)**
1.5	2.915	2.938	-0.8
5.0	2.411	2.450	-1.6
10.0	1.796	1.814	-1.0
15.0	1.316	1.334	-1.4
20.0	0.972	0.984	-1.2

10x10 cm^2 field			
Depth (cm)	**Film dose (Gy)**	**TPS dose (Gy)**	**Diff. from TPS (%)**
1.5	3.079	3.084	-0.2
5.0	2.606	2.629	-0.9
10.0	1.991	2.014	-1.2
15.0	1.515	1.519	-0.3
20.0	1.148	1.143	0.5

20x20 cm^2 field			
Depth (cm)	**Film dose (Gy)**	**TPS dose (Gy)**	**Diff. from TPS (%)**
1.5	3.297	3.229	2.1
5.0	2.849	2.819	1.1
10.0	2.246	2.223	1.0
15.0	1.796	1.727	4.0
20.0	1.397	1.327	5.2

Table 2. The results of absolute dose measurements with the film perpendicular to the beam direction for five different depths. Also listed are the calculated doses from the TPS (Helax-TMS) and the percentage difference between film and the TPS calculated from $(D_{meas.}-D_{calc.})/D_{calc.}x100$.

The ICRU Report 42 (ICRU 1987) recommends accuracy for dose calculations of ±2% or, alternatively ±2 mm in very steep dose gradient regions where there is a change of greater than 10% of average intensity per centimetre. Venselaar *et al.* 2001 have proposed values of tolerances according to Table 3. Mijnheer *et al.* have suggested the same tolerances according to Venselaar *et al.* 2001 in a coming ESTRO booklet (ESTRO Booklet No. 7). These tolerance values are summarized below in Table 3.

Figure 19 shows the registered absorbed dose distribution by the film for a 10x10 cm^2 field at 10 cm depth (a) and the calculated dose distribution (b). The agreement between the dose distributions seems qualitatively to be very good. A problem with the used software for analysis is that it is not possible to display the dose distributions in absolute doses, despite the fact that the film is scanned and converted to absolute dose by the software. The dose plans must be normalized, for example, to a maximum dose within a region of interest (ROI), or to a specific cursor position. We have tried to match the normalization doses as close as possible without losing the absolute dose difference between measurement and calculation. The dose levels used for normalisation are indicated in the upper right corner in Figure 19 a) and b), respectively. Dose profiles through the centre of the field in the two principal directions are shown in Figure 19 c) and d).

Region		Homogenous, simple geometry	Complex geometry (wedge, inhomogeneity, asymmetry, blocks / MLC)	More complex geometries****
δ_1	*Central beam axis data* – high dose, low dose gradient	2%	3%	4%
δ_2*	*Build-up region of central axis beam, penumbra region of the profiles*- high dose, high dose gradient	2 mm or 10%	3 mm or 15%	3 mm or 15%
δ_3	*Outside central beam axis region*- high dose, low dose gradient	3%	3%	4%
δ_4**	*Outside beam edges* – low dose, low dose gradient	30% (3%)	40% (4%)	50% (5%)
RW_{50} ***	*Radiological width* –width of a profile measured at half its height compared to the value at the beam axis.	2 mm or 1%	2 mm or 1%	2 mm or 1%
δ_{50-90}	*Beam fringe* – distance between the 50% and the 90% relative to the maximum of the profile in the penumbra	2 mm	3 mm	3 mm

Table 3. Recommended tolerances (δ) for various regions in a photon beam (from Venselaar *et al.* 2001).

* One of the two tolerance values should be used.
** These figures are normalized to the local dose, or at the dose at a point at the same depth on the central beam axis (in brackets).
*** The percentage figure should be used for field sizes larger than 20 cm.
****More complex geometry is defined as a combination of two or more complex geometries.

According to the tolerance values proposed by Venselaar *et al.* 2001 for homogeneous simple fields, the penumbra region should be within 2 mm or 10%. By just studying the profiles by eye it is hard to say, especially in the z-direction in the penumbra region, if the result is within the tolerance. A gamma evaluation with 2% and 2 mm criteria is shown in Figure 19 f), revealing that it is only in the penumbra region that acceptance fails. The colours of the palette range are set to be white for 100% ($\gamma = 1$), and accepted regions are white and blue. Regions that fail are shown in red. The regions that fail, i.e. the penumbra, can partly be due to the difficulties to match the origins and the exact sizes of the fields on the film and in the TPS. The gamma evaluation method is not a good tool for evaluation of low dose regions, where the calculation can fail though it is within the set criteria. For example if we are comparing two dose points of 4% and 1% dose, and the dose criteria is set to be 2%, this will lead to a gamma value larger than 1 ((4%-1%)/2%). The 3% dose difference can still be within acceptable tolerances but the gamma calculation fails. Measured (solid lines) and calculated (dashed lines) isodose distributions are shown in Figure 19 e). The 10% isodose lines are the ones that differ most, but again this is in the penumbra region.

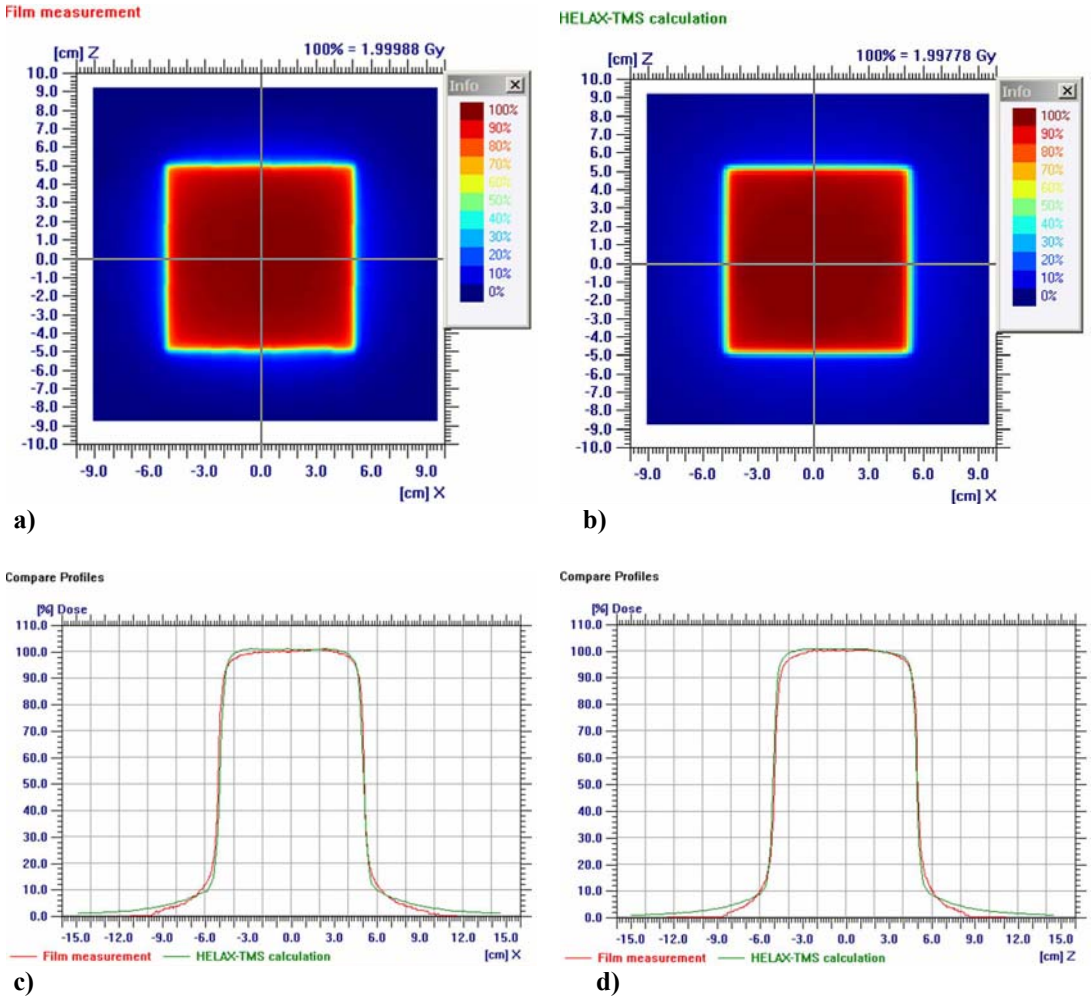

Figure 19. Comparison between TPS calculated and measured absorbed dose distributions with the film oriented perpendicular to the beam axis for a 10x10 cm^2 field, 6 MV photon energy. a) Absorbed dose distribution from film measurement, b) dose distribution calculated in the TPS, c) dose profile along the x-direction through the centre of the field, d) dose profile along the z-direction through the centre of the field

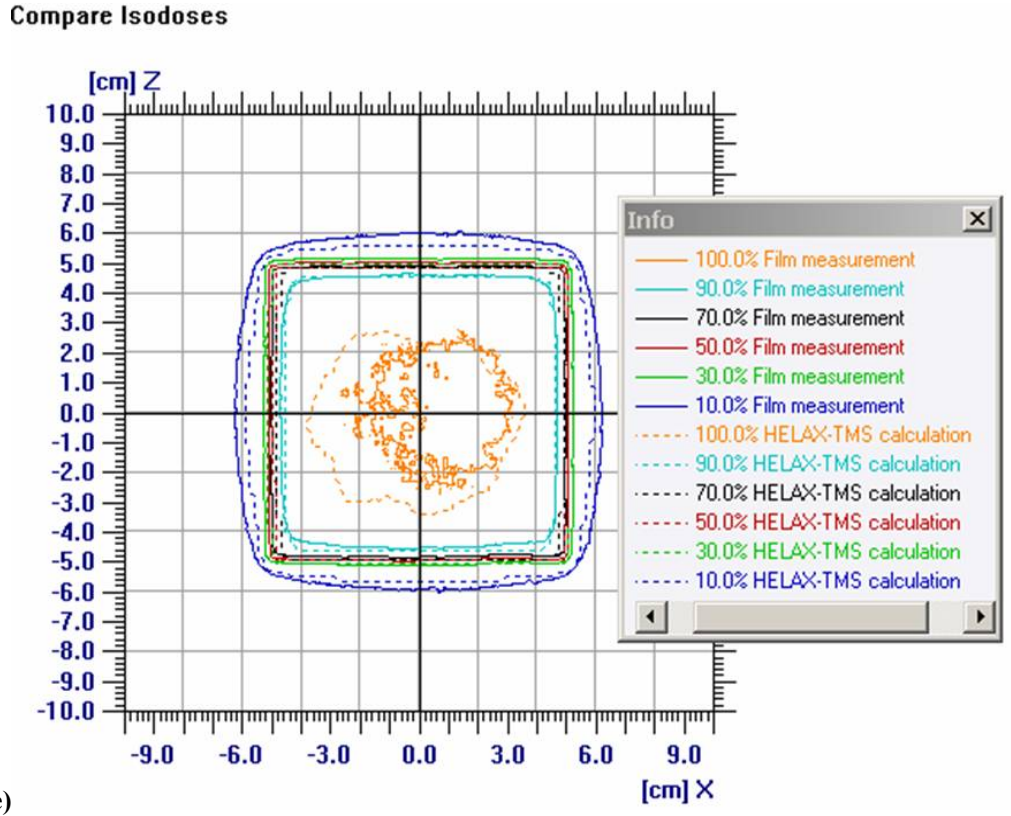

e)

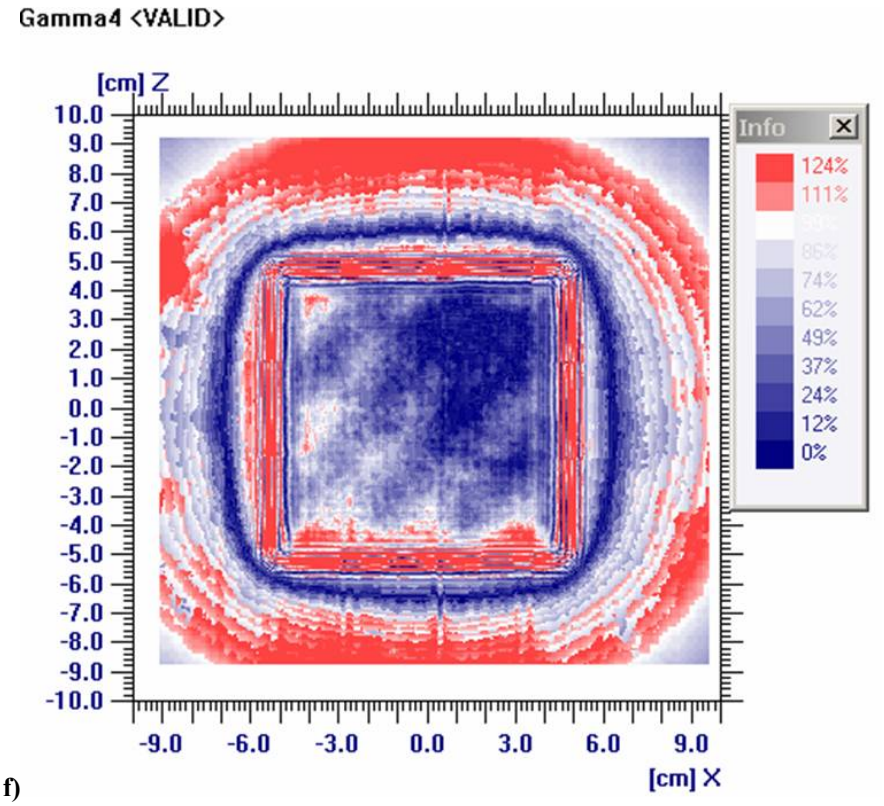

f)

Figure 19. Comparison between TPS calculated and measured absorbed dose distributions with the film oriented perpendicular to the beam axis for a 10x10 cm^2 field, 6 MV photon energy. e) isodose comparison between film measurement and TPS calculation, f) gamma evaluation for measurement and calculation (pass-fail criteria 2% and 2 mm).

- **Single quadratic beams, film oriented parallel to the radiation beam axis**
  To study the properties of the film when it is positioned parallel to the propagation of the beam, a depth dose curve (in absolute dose) was determined. Comparison of absorbed dose measured with the film in polystyrene, with a diode in water and calculated by the TPS in polystyrene is presented in Figure 20.

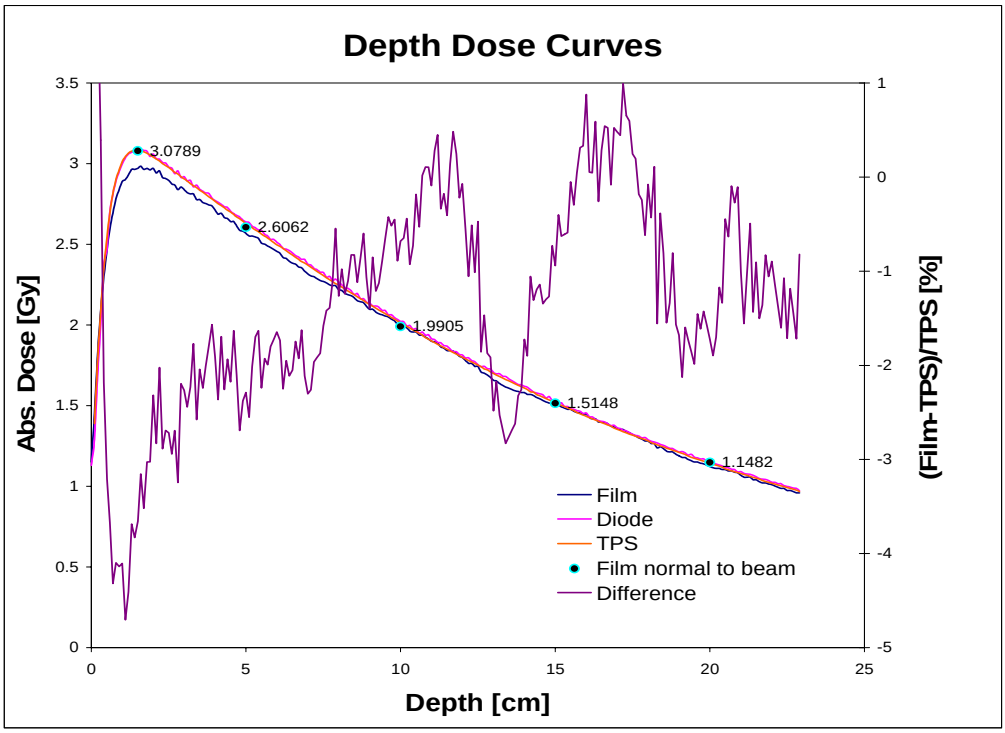

Figure 20. Depth dose curves measured with film (blue colour) positioned parallel to the central beam axis, diode (pink colour) and calculated by the TPS (orange colour). The point doses measured with film oriented normal to the beam axis are also shown. The percentage difference between the film and calculation is also shown with its corresponding vertical axis to the right.

Figure 20 shows that the diode measurements scanned in a water tank and the depth dose calculated by the TPS coincide with one another and are hardly distinguishable. This persuades us to believe that, if we can verify our film dosimetry with either our TPS or the diode dosimetry, it will also be in agreement with the other. In Figure 20 the film measurement shows a depth dose for the film parallel to the central beam axis. Note that the film was not placed in the central axis but 0.5 cm off-axis to avoid attenuation from the film itself. The vertical axis to the right corresponds to the deviation of the film from the TPS. The deviation is within 2% except in the build-up region and at a depth around 13-14 cm (within 3 %) where there is a small dip in the depth dose for the film (probably due to some local fault in the film or the phantom). In clinical cases where we want to verify the doses delivered to the target and the OARs, the depths we are dealing with are normally deeper than the dose maximum. Therefore our film dosimetry shouldn't hinder us from using it since it is only in the build-up region where the deviation is significant. Also plotted in the diagram are the point doses measured with the film normal to the incident beam. Data measured with the film normal to the beam agrees very well with our TPS calculations and diode measurements. The EDR2 film can

be used to accurately measure absolute dose within 2% to a depth of at least 23 cm, ignoring the build-up region, with the film oriented parallel to the incident beam. In a patient case, the CT scans are in the axial plane. The dose matrices are therefore usually in the axial plane in the TPS, and to verify these dose distributions in the axial plane we will have to orient the film in this plane in the phantom.

- **Multiple quadratic beams, film oriented parallel to the radiation beam axis**

  We have shown that the EDR2 film, positioned either normal or parallel to the beam axis, can be used for accurate verification of simple open quadratic single fields. The next step is to combine several fields and to check if the accuracy of the film measurements is maintained. Two cases have been studied, a two-field opposing technique and a four-field box technique, both delivered to the CarPet phantom. The results from the film measurements are analyzed and compared with calculated dose matrices in the same manner as described above. Figure 21 shows the result for the two-field case. Figures 21 a) and b) show the measured and TPS calculated dose distributions, respectively. By eye, they seem to be quite similar. Figures 21 c) and d) show the profiles along the centre in the x and z-directions, sinister-dexter and anterior-posterior (sin-dx and AP), respectively, if the patient would be lying on the couch on his/her back. The red profile, which represents the measurement with film, is slightly higher than the green profile from the calculation, especially near the beam entrances. Figure 21 e) shows the isodose distributions where solid lines represent film measurement and dashed lines the calculation. The agreement between measurements and calculations is qualitatively very good. A quantitative comparison is shown in Figure 21 f) using the gamma evaluation method where white and blue regions indicate that the gamma calculation passes the criteria of 2% and 2 mm. The only locations that do not pass these criteria are the build-up area and the penumbra region. Except for real deviations in these regions the discrepancies might to some extent be due to difficulties in exact matching of the origins of the film and of the calculated dose matrix. Another reason to the discrepancy is that TPS calculations in the build up region are inaccurate (Knöös *et al.* 1994). Deviations in the penumbra region could also depend on that the TPS uses nominal field sizes while the field size of the accelerator can differ from time to time from the correct size.

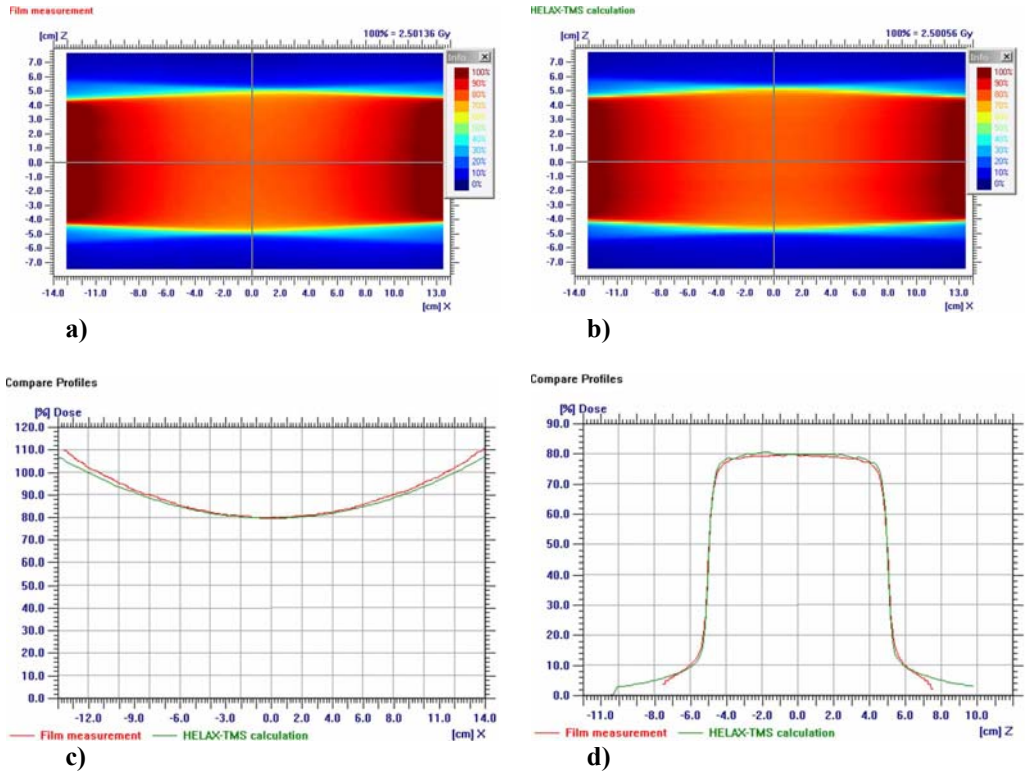

Figure 21. Two opposing lateral fields delivered to the CarPet phantom. a) Absorbed dose distribution measured with film, b) calculated dose distribution in the TPS, c) dose profile in the centre of the beam along the x-direction, sinister-dexter (sin-dx), d) dose profile in the centre of the beam along the z-direction anterior-posterior (AP).

e)

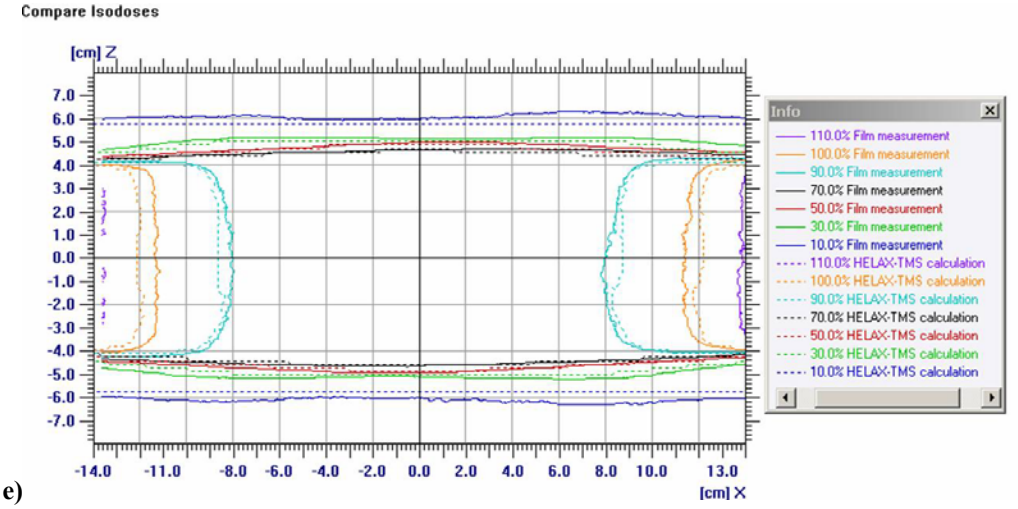

f)

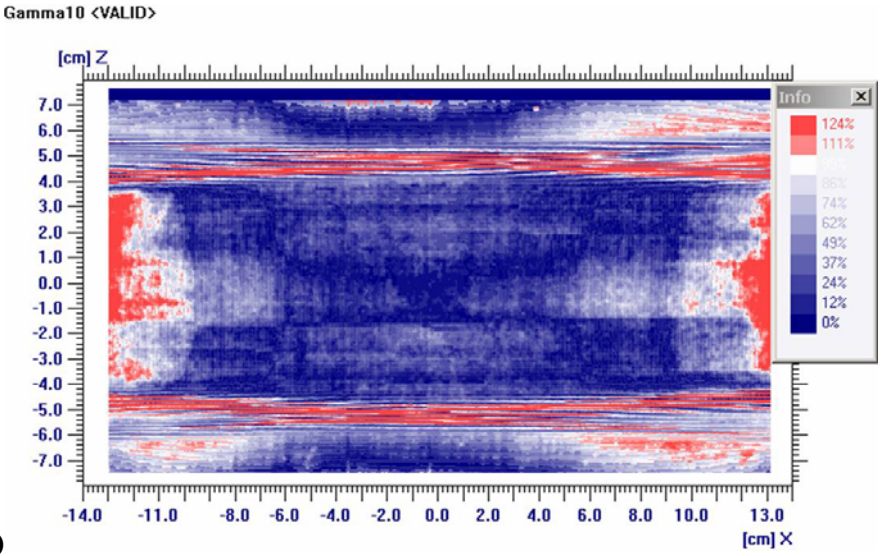

Figure 21. Two opposing lateral fields delivered to the CarPet phantom. e) comparison of isodose distributions, f) gamma evaluation (pass-fail criteria 2% and 2 mm).

Figure 22 shows the corresponding results for the four-field box. Even this somewhat more complex case demonstrates good agreement at least in the area where the beams intersect. The criteria of 2 mm and 2% are chosen from Table 3, even though these criteria are set to evaluate either only the DTA or only the dose difference. The gamma evaluation combines these to ways of evaluation and one might consider other criteria then.

In Figure 22 f), the gamma calculation outside the field (green area in Figure 22 a) and b)) where the absorbed dose is at least 1 Gy the calculation can not pass the set criteria of 2% and 2 mm.

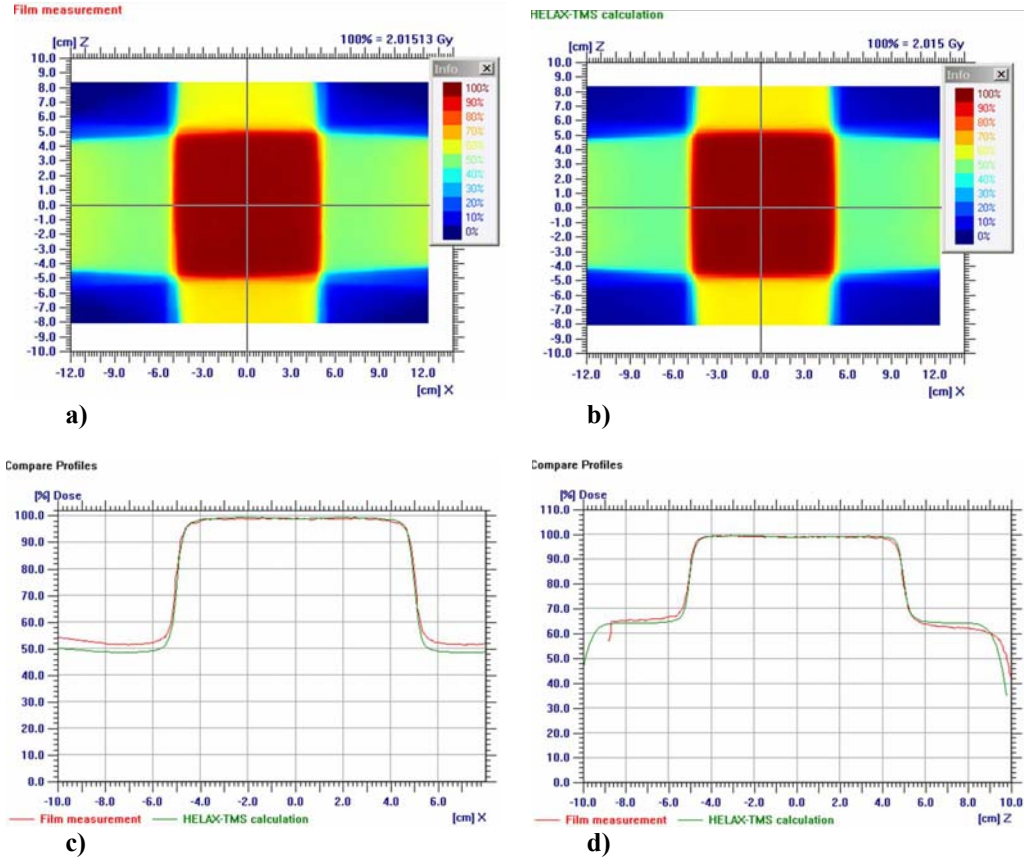

Figure 22. A four-field box delivered to the CarPet phantom. a) Absorbed dose distribution measured with film, b) calculated dose distribution in the TPS, c) dose profile in the centre of the beam along the x-direction (sin-dx), d) dose profile in the centre of the beam along the z-direction (AP).

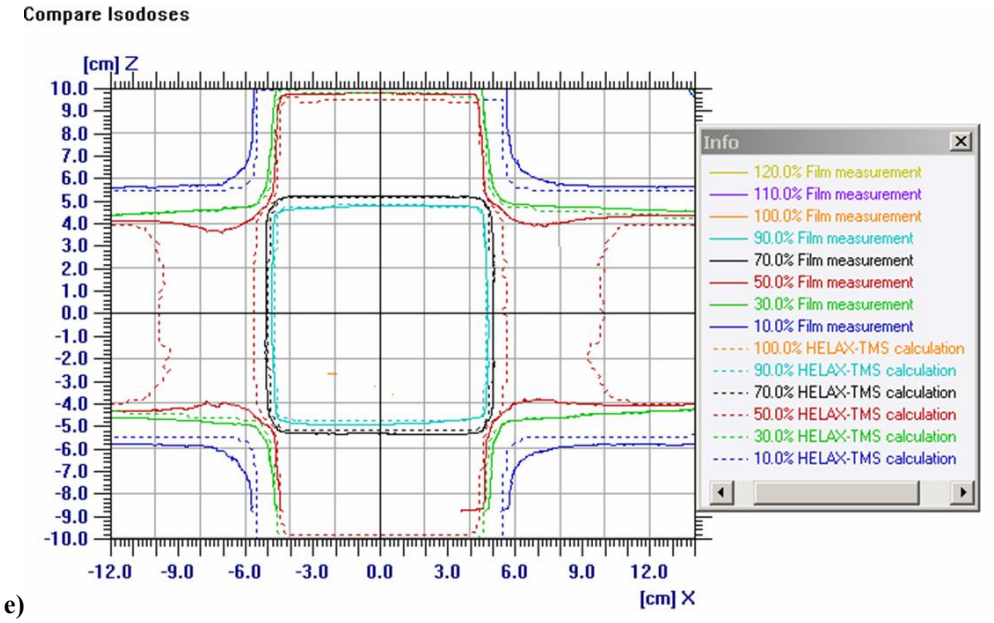

e)

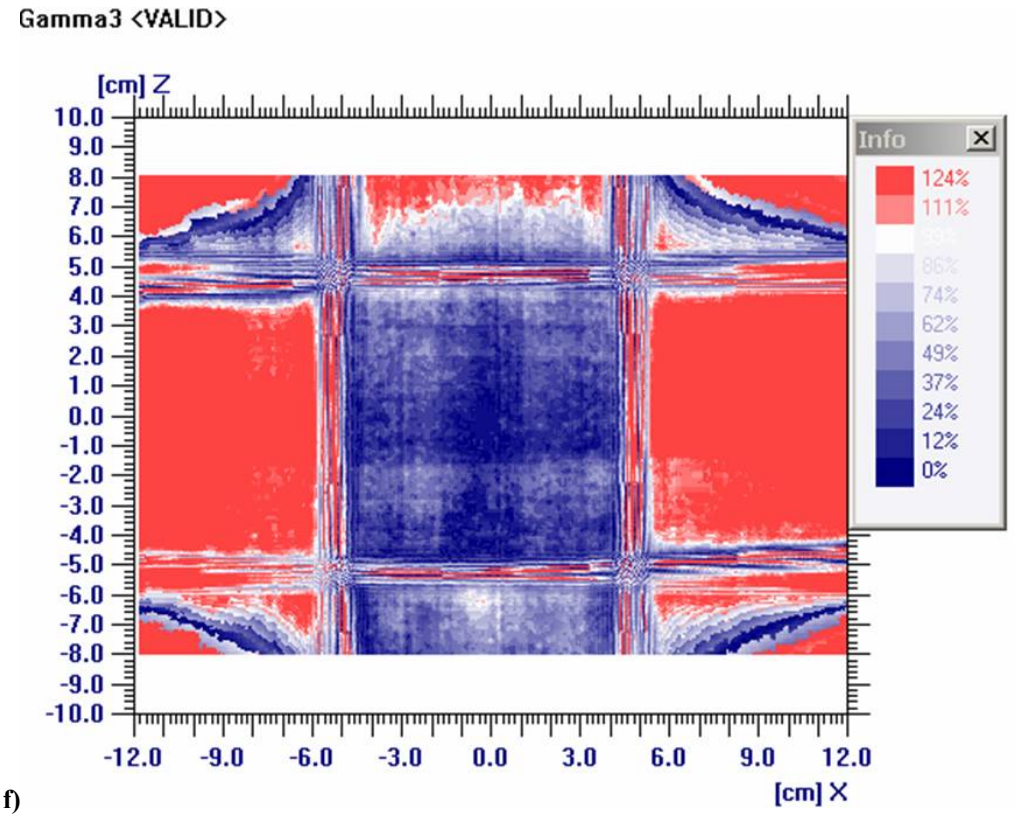

f)

Figure 22. A four-field box delivered to the CarPet phantom. e) isodose distributions, f) gamma evaluation (pass-fail criteria 2% and 2 mm).

- **Verification of intensity modulated beams**
  Each field from an IMRT plan on the CarPet phantom was verified individually with the film positioned perpendicular to the incident beam. The results are presented in Figure 23. It is obvious that there are some rather large discrepancies between measurements and calculations in the low dose areas. The discrepancies can depend on that the delivered dose does not agree with

the TPS calculated dose, which will have larger consequences especially in the low dose areas. This in turn can lead to larger discrepancies in the film measurement in the low dose areas. The profile in Figure 23 c) is along the sin-dx direction in the high dose area at about z = -4, and the profile in d) is along the centre of the beam in the AP-direction. These profiles agree reasonably well in the high dose areas but differ significantly in the low dose regions. Only data for beam number one in the treatment plan is shown in Figure 23, but all other beams show similar results. The discrepancies between measurements and calculations are revealed in the gamma calculation in Figure 23 f). This might partly depend on that the gamma evaluation is not a good method in low dose areas. A possible improvement to this problem would be to increase the number of MU per field but with the drawback that this does then not simulate the real beam delivered to the patient. IMRT is still in its infancy and rapidly evolving. Because of the rapidly changing nature of IMRT there are no firm recommendations of tolerances for IMRT. At present, there are no published dosimetric criteria for IMRT treatments (Cadman *et al.* 2002).

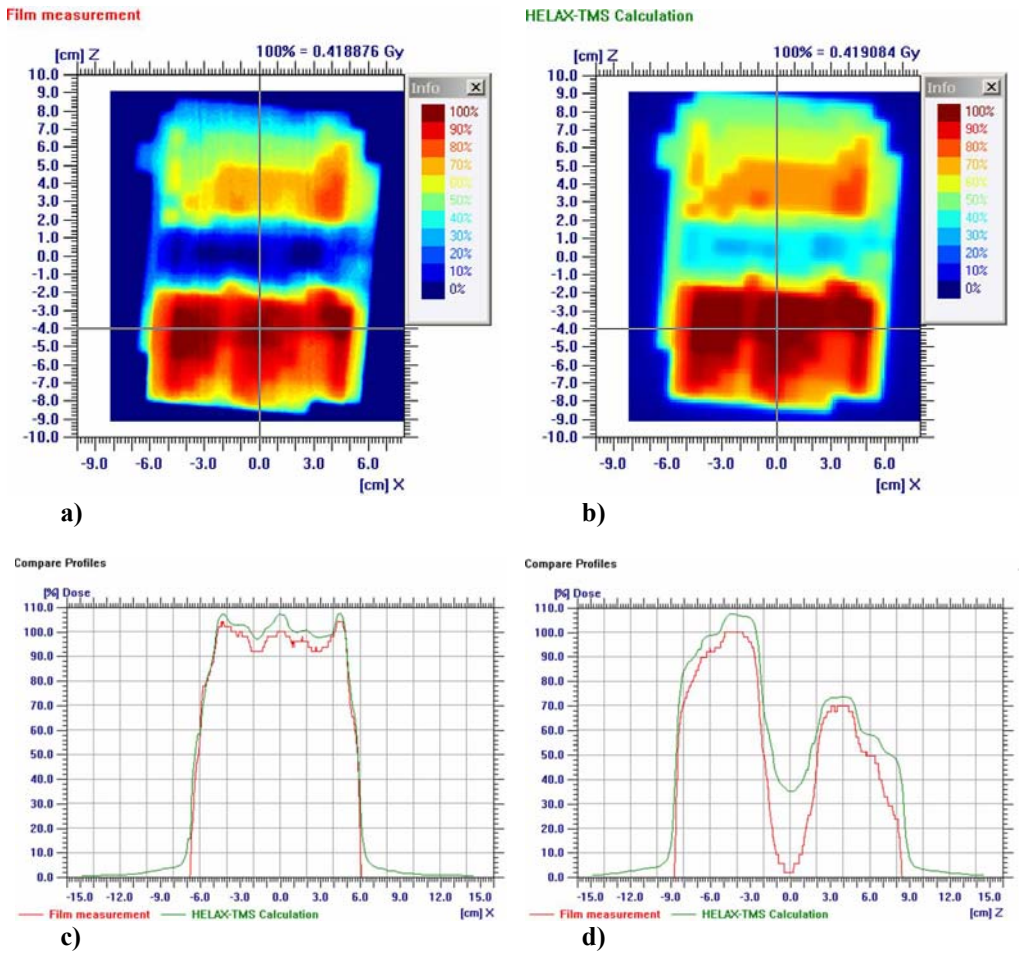

Figure 23. Verification of a single intensity modulated beam in the CarPet phantom with a film positioned perpendicular to the radiation beam axis. The result for beam number 1 in the treatment plan is shown. a) Measured absorbed dose distribution, b) planned dose distribution in the TPS, c) dose profile at z = -4 along the x-direction (sin-dx), d) dose profile in the centre along the z-direction (AP).

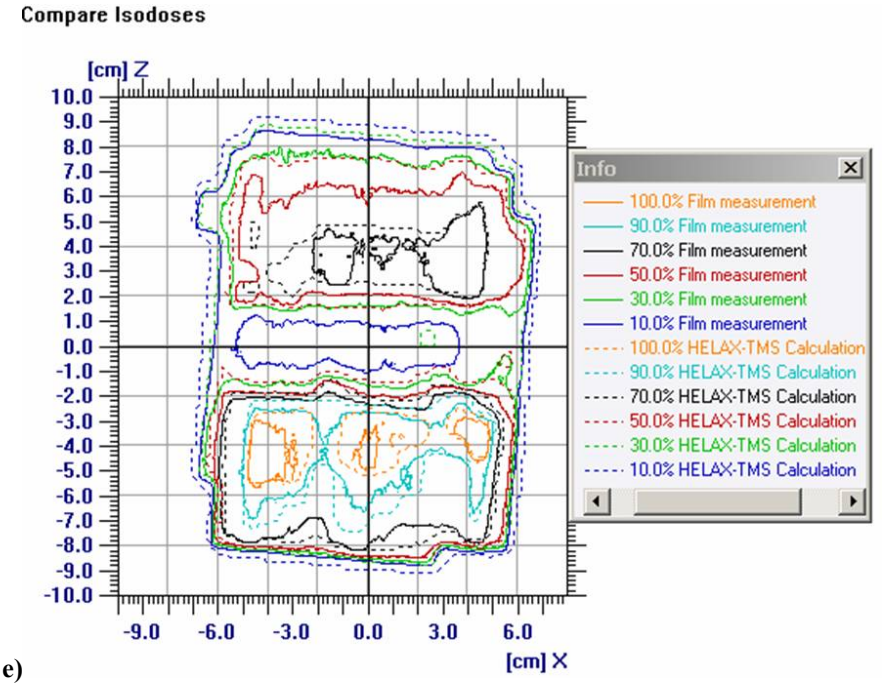

e)

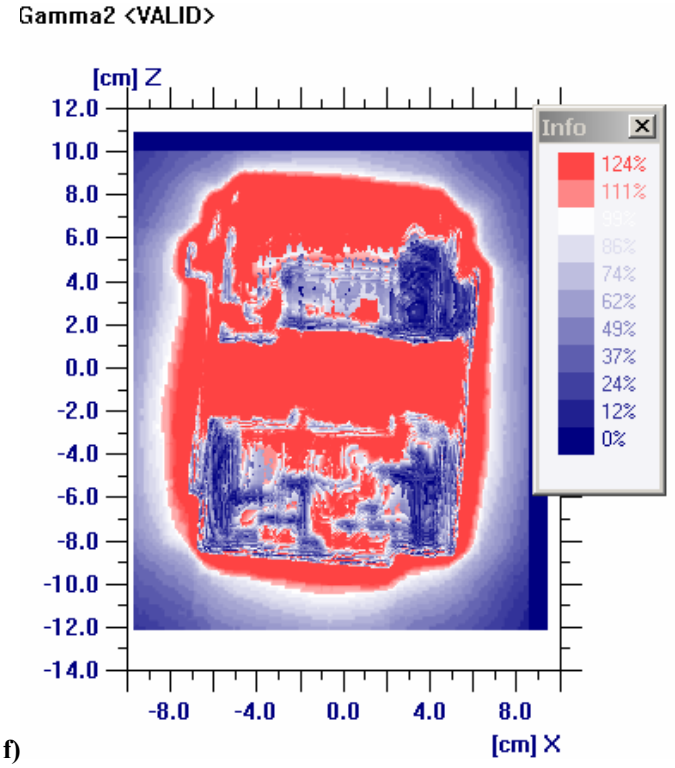

f)

Figure 23. Verification of a single intensity modulated beam in the CarPet phantom with a film positioned perpendicular to the radiation beam axis. The result for beam number 1 in the treatment plan is shown. e) isodose distributions, f) gamma evaluation (pass-fail criteria 4% and 3 mm).

- **Verification of an IMRT plan for a phantom case**
  An IMRT plan for the PTV/OAR in the CarPet phantom was optimised and recalculated in our two TPSs according to the method described by Ambolt (2004). This plan participates in an European study where the same geometry and dose criteria are used in several different environments. All plans determined locally are irradiated in the CarPet phantom using films from a

central distribution site. These films are sent back to the centre, developed, scanned and analysed in a similar way for all sites participants in the study. We have used this opportunity to benchmark our dosimetry methods for IMRT.

The resulting plan had nine fields with a total of 120 segments. The plan was verified with films positioned in the CarPet phantom and analyzed according to the method outlined in this study. The results presented in Figure 24 are from the film positioned at 1 cm off-axis (towards the feet of a patient). The other films taken at the other locations are not presented. Figure 24 a) and b) show the dose distribution on the film and in the TPS respectively. Figure c) and d) show the corresponding profiles along the lines in a) and b), and Figure 24 e) shows the isodose distributions. The gamma calculation in Figure 24 f) shows convincing result in at least the target and in the OAR area. Outside the target and the OAR, on the other hand, the agreement becomes worse. One reason might be that the criteria (3%, 3 mm) are set unrealistically tight for the step-and-shoot technique. Further investigations are needed to settle the exact reason for this.

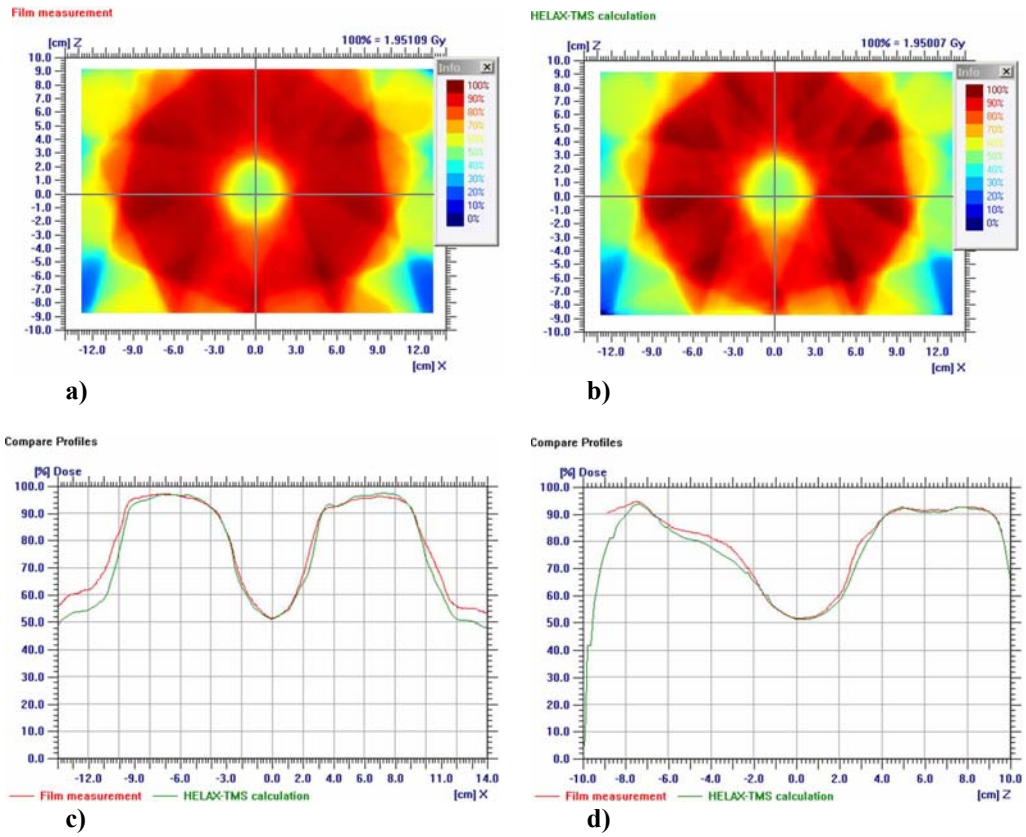

Figure 24. An IMRT phantom case optimized in OTP and forward calculated in Helax-TMS. a) Absorbed dose distribution measured with film, b) calculated dose distribution in the TPS, c) dose profile in the centre of the beam along the x-direction (sin-dx), d) dose profile in the centre of the beam along the z-direction (AP).

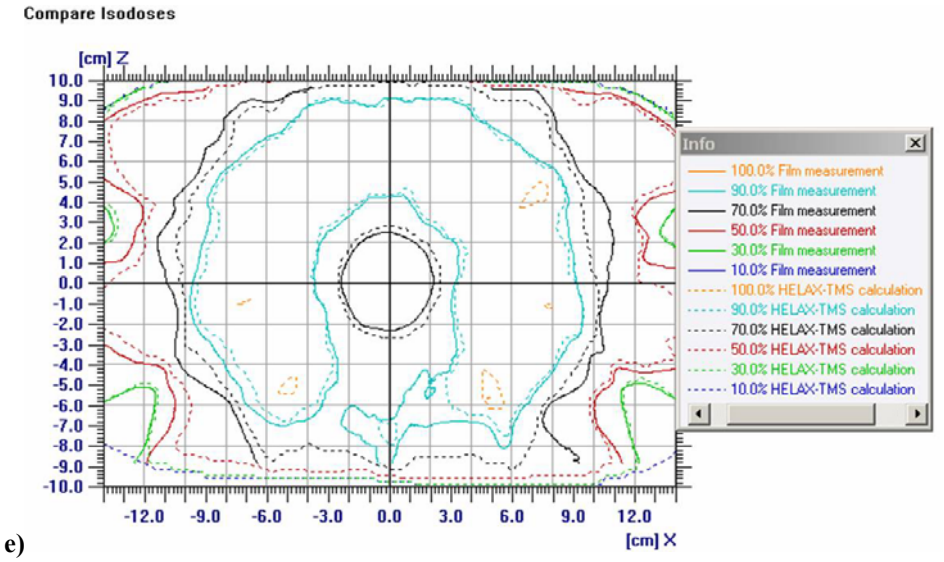

e)

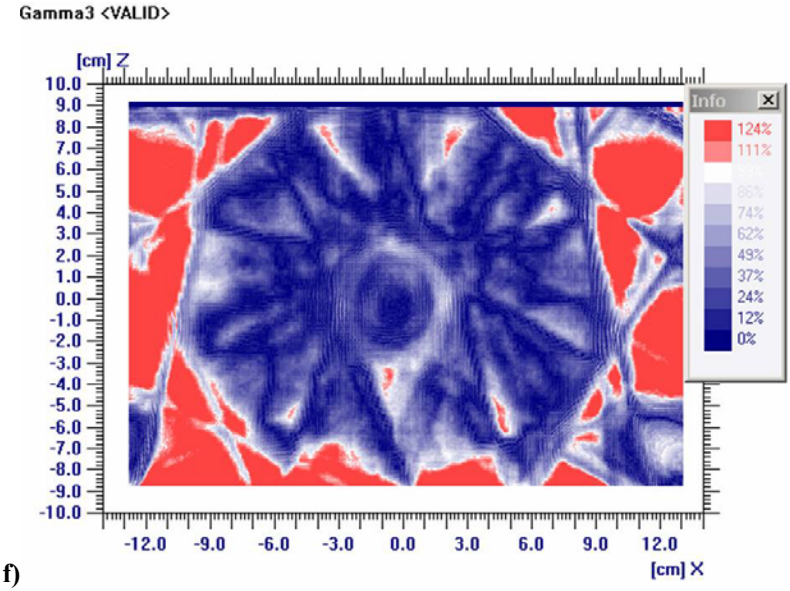

f)

Figure 24. An IMRT phantom case optimized in OTP and forward calculated in Helax-TMS. e) isodose distributions, f) gamma evaluation (pass-fail criteria 3% and 3 mm).

The films taken at the other locations of the phantom show about the same agreement and are not presented here.

Verification of an IMRT plan for a patient case

A 61 year old male patient, with the diagnosis squamous cell carcinoma of the tonsil with lymph node metastases, was optimized in OTP and forward calculated in Helax-TMS. Seven fields were used with a total of 52 segments. The results presented in Figure 25 indicate quite good agreement between measured and TPS calculated doses. The result is from the film placed 1 cm off-axis towards the head of the patient. Figures 25 a) – e) show the dose distributions, profiles and isodose distributions. In Figure 25 f) it is shown that the gamma calculation passes the set criteria (3%, 3 mm) in most areas, with a few exceptions. Especially in regions with nonhomogenous dose distribution, where many fields intersect, the pass-fail criteria are not always fulfilled. But the result of the plan is after all quite good.

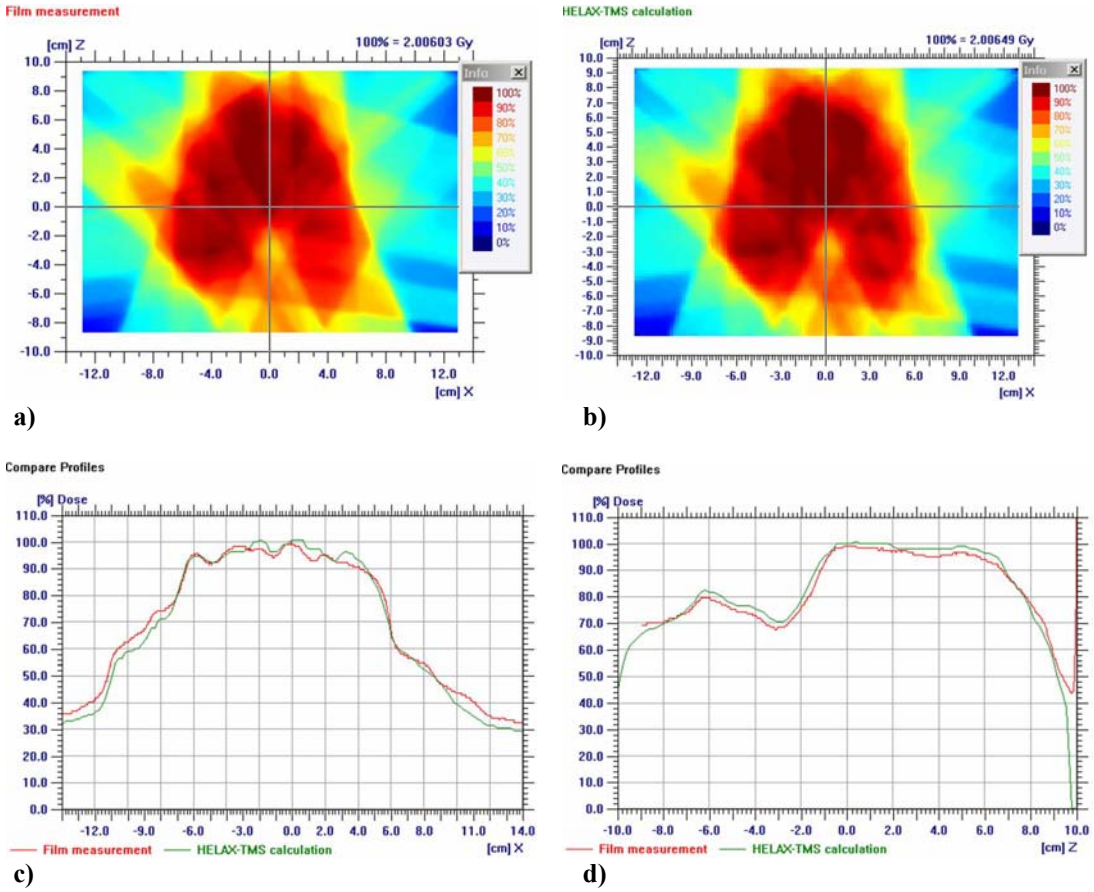

Figure 25. An IMRT clinical patient case optimized in OTP and forward calculated in the TPS. a) Absorbed dose distribution measured with film, b) calculated dose distribution in the TPS, c) dose profile in the centre of the beam along the x-direction (sin-dx), d) dose profile in the centre of the beam along the z-direction (AP).

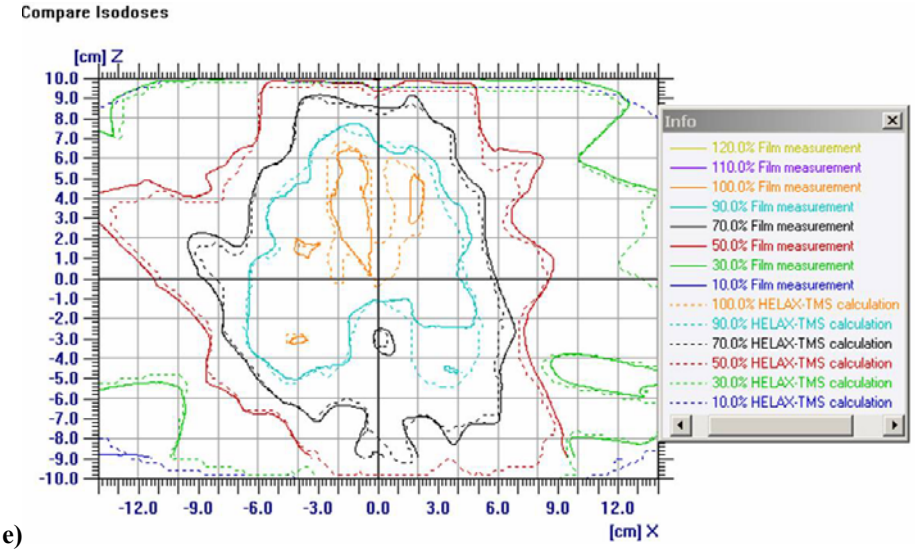

e)

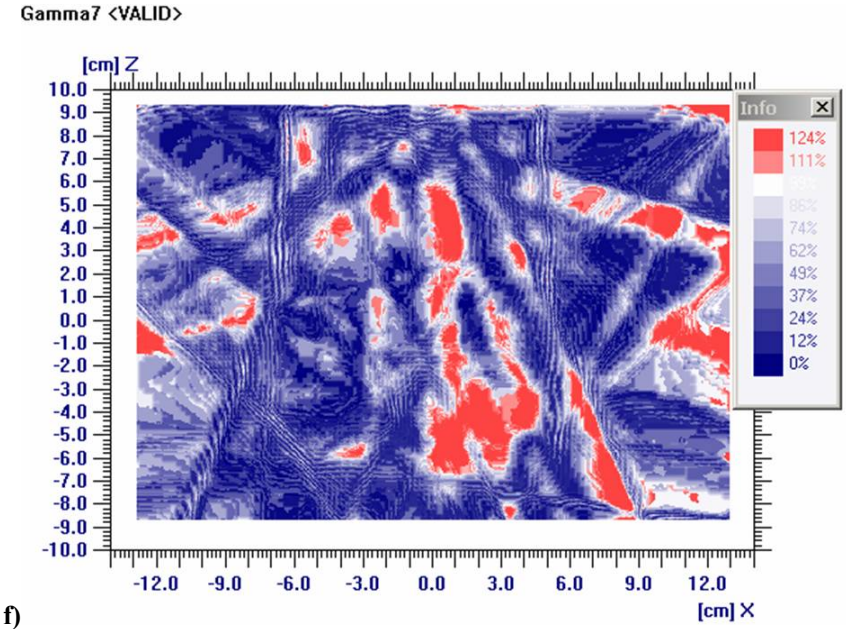

f)

Figure 25. An IMRT clinical patient case optimized in OTP and forward calculated in the TPS. e) isodose distributions, f) gamma evaluation (pass-fail criteria 3% and 3 mm).

Absolute dose measurements with ion chamber and TLD

In the phantom case described above the absolute dose to the target and the OAR were also measured with an ionisation chamber and compared with calculations from the TPS. Table 4 shows data from the ion chamber measurements. Each beam was delivered with the planned gantry angle, i.e. the phantom was irradiated from nine different directions. The registered charges from each beam were noted and the total charge from all beams were added together and divided with the charge corresponding to 1 Gy to the isocentre in an open 10x10 cm^2 field. The charge collected from the open field in the isocentre was 22.37 nC (average of three measurements). Ion chamber measurement was also performed for the patient case (see Table 5) where the charge corresponding to 1 Gy to the isocentre for an open 10x10 cm^2 field was 22.15 nC. Table 6 summarizes the absolute doses for calculation and measurement.

	OAR		TARGET	
Field nr	Ion chamber (Gy)	TPS	Ion chamber (Gy)	TPS
1	0.10	0.09	0.12	0.11
2	0.09	0.08	0.26	0.23
3	0.11	0.11	0.25	0.23
4	0.13	0.13	0.22	0.20
5	0.19	0.18	0.19	0.20
6	0.13	0.13	0.20	0.16
7	0.12	0.11	0.23	0.22
8	0.10	0.09	0.24	0.22
9	0.09	0.09	0.23	0.23
Total dose:	**1.08**	**1.00**	**1.94**	**1.81**

Table 4. Absorbed dose measured with ion chamber and TPS calculated dose for each field for the phantom case. The total dose is shown in the bottom row.

	TARGET	
Field nr	Ion chamber (Gy)	TPS
1	0.26	0.13
2	0.21	0.11
3	0.24	0.13
4	0.30	0.15
5	0.25	0.13
6	0.22	0.11
7	0.41	0.25
Total dose:	**1.92**	**2.00**

Table 5. Absorbed dose measured with ion chamber and TPS calculated dose for each field for the patient head and neck case. The total dose is shown in the bottom row.

	TPS	Film	Ion chamber	TLD
Abs. Dose in target (Gy): (Phantom case)	1.81	1.80 -1%	1.94 7%	
Abs. Dose in OAR (Gy): (Phantom case)	1.00	1.01 1%	1.08 8%	
Abs. Dose in target (Gy): (Patient case)	2.00	1.99 0%	1.92 -4%	2.03 1.4%

Table 6. Summary of TPS calculated dose and measured absorbed dose with film and ion chamber, and also complemented with a TLD measurement for the patient head and neck case. The percentage figures represent the difference between measured and calculated values.

According to Table 6, the TPS and the measurements with film agree very well, within 1%. The ion chamber measurement, however, differ with up to 8%. This persuades us to believe that there exist problems when measuring the absolute dose to a point with an ion chamber. The absorbed doses measured with the ion chambers are both higher and lower compared to the TPS calculated doses, showing no consistency. The experiment was repeated showing the same result. A TLD measurement was also performed for the patient case which differed with only 1.4%. The method to measure the absolute dose with the TLDs was performed similar as with the ion chamber. The readings of the TLDs were referred to an open 10x10 cm^2 field with 1 Gy to the isocentre.

A similar test was performed with the four-field box plan with open square fields, 10x10 cm^2 fields, and the prescribed dose was 2 Gy to the isocentre. The results from this experiment are shown in Table 7.

Gantry angle	*Ion chamber (Gy)*	*TLD (Gy)*
0°	0.56	
90°	0.44	
180°	0.56	
270°	0.44	
Total Dose:	**2.008**	**2.043**

Table 7. Absolute dose measurement with ion chamber and TLD for a four-field box with open square 10x10 cm^2 fields.

From Table 7 we can see that the absolute dose from the ion chamber only differs with 0.4% from the calculated value. The measurement was complemented with TLD measurements and the reading differed with 2% from the TPS. The absolute dose measurements with the ion chamber is hence in excellent agreement with calculated data for open quadratic fields but rather large discrepancies are present when it comes to IMRT. In our IMRT setting, the step-and-shoot technique is executed with a "static sliding window" technique. This means that the segments within one field start at one side and "slides" over to the other side in a static manner. Some segments in the IMRT plan are quite small and partial irradiation of the ion chamber is rather common which might be one reason for the large discrepancy found for the ion chamber measurements.

It has been reported in the literature that differences of more than 6% can be found for Farmer chamber measurements in IMRT fields (Laub *et al.* 2003). The 0.6 cm^3 Farmer chamber has a relatively large measuring volume. Since the segments can be small in IMRT and the measuring cavity is large, high dose gradients in the proximity and/or even along the cavity can lead to an over- or underestimation of dose values. This volume effect of the Farmer chamber could lead to inaccuracy in the verification of absolute point dose measurements in IMRT. There is a developing consensus, when it comes to measurements with ion chambers in phantoms in IMRT that, a reasonable action level in high dose, low gradient regions is 3- 4%. The reason for this is that small fields and localized gradients may cause additional uncertainties in some cases (Ezzell *et al.* 2003).

Leybovich *et al.* 2003 claim that when using large ion chambers such as 0.6 cm^3 chambers, the electron fluence through them may not be uniform. Thus, an ion chamber's collecting volume may be partially irradiated at a given moment. Even when the entire volume is irradiated, the fluence distribution may not be uniform due to nonuniform beam profiles. However when the entire IMRT field sequence is delivered, the dose distribution in the target will be reasonably uniform as indicated by the calculated IMRT dose distribution. Thus, uniformity may be achieved at the location of the ion chamber when all the fields from the IMRT plan are delivered. Leybovich *et al.* 2003 also demonstrated that as long as the ion chamber is positioned in an area with reasonably uniform dose distribution, spatial fluence uniformity would exist in the chamber's collecting volume and the dose measured by a chamber would not be affected by its dimensions. When using the 0.6 cm^3 chamber, the measured absorbed dose compared to the calculated dose was within 0.5%. This is something we could not achieve with our step-and-shoot technique for our particular IMRT plan, though the chamber was positioned in areas with very homogeneous dose distribution.

One actually has to question this conclusion that, as long as the accumulated dose distribution is homogenous, Farmer chambers can be used. It must be the relative number of segments that partially irradiate the chamber that matters and their relative contribution to the total dose that is of importance. If the number of segments is small one can use Farmer type chambers, but in cases where a large proportion of segments partially irradiate the chamber problems might occur. This was also shown in our two cases where the Quasimodo case had larger discrepancies than the patient case, the latter having fewer segments.

Van Esch *et al*. 2002 compared results of acceptance tests and quality control procedures from five different clinics. They used pass-fail criteria for the gamma evaluation of 3% and 2 mm with good results. Plans were accepted if only small areas exceeded the criteria. The largest deviation for the absolute dose on the beam axis within the span of the used parameter values was 3.7%. All clinics, however, used the sliding window technique with dMLC. Adams *et al*. 2003 have implemented IMRT at the Royal Mardsden using both dMLC and sMLC. Measurements of relative dose distributions generally showed agreement with the planning system to within 3% and 3 mm, with mean absolute dose measurements agreeing within 2%. For the step-and-shoot technique they have used Helax-TMS as the planning system and the ion chamber used for absolute dose measurement was a NE2571.

Price *et al.* 2003, have compared the measured (0.125 cm^3 PTW ion chamber) and calculated phantom dose measurements for over 1000 patients treated with the sMLC-technique. The equipments used were the Siemens Primus or the Primart linear accelerators. The following statistics are from their study:

39.3% of patients within ±1%
69.7% of patients within ±2%
93.7% of patients within ±3%
6.3% of patients > 3%
0.8% of patients > 4%

IMRT delivery with the step-and-shoot technique

The total radiation delivery time, delivered through the Oncentra-Visir record-and-verify system, for irradiation of the CarPet phantom was around 40 minutes. This is a too long delivery time and not clinically acceptable. Besides, we never accomplished to deliver a whole plan without any stops or failures. The exact reason for these practical problems is unknown. If it depends on record and verification system, the accelerator or the connection in between is yet unknown. Some possible explanations can be that there are too many segments with very few MUs.

The total irradiation time for the patient case was around 15 minutes. This is clinically realizable. In addition, the whole plan was in this case delivered without any stops or failures. The reason might be that this case had fewer segments and segments with more MUs per segment compared to the phantom case described above.

IV. CONCLUSION

A film dosimetry method for IMRT dose verification has been evaluated. The goal was to find a reliable verification system to check that the delivered doses agreed with TPS calculated doses. The method utilizes the EDR2 films, which evaluated with appropriate software, have shown to meet these demands within certain tolerances, but not in all cases. Relative 2D dose distributions and also absolute dose measurements are acceptable within certain depths. Especially when the film is oriented normal to the beam it measures very accurately. Depth doses measured with film in polystyrene, TPS calculations, and diode measurements in water agreed within 2% to a depth of 23 cm ignoring the build-up region. These results indicate that, with proper care, the film system can be used to accurately measure absolute dose in a phantom when oriented parallel to the incident beam.

The results from the ion chamber measurements are very poor for the IMRT cases and the reason for this should be further investigated. Studies should be directed to investigate how the number of intensity levels, number of segments and the size of the segments can affect the accuracy of the ion chamber measurements in the step-and-shoot technique. Alternative dosimeters, TLDs, were used to complement the measurements. The results from the TLDs reinforced the suspicion that there is a problem with the ion chamber measurements in IMRT.

The QA procedure to check each IMRT patient with phantom measurement before the first treatment is demanding and workload intensive. But radiographic film does still have very good spatial resolution and cannot be replaced fully yet. The use of radiochromic film for IMRT verification is today not accurate enough and not economically feasible. To use radiochromic film as a substitute for radiographic film, the radiochromic film needs to get rid of all the problems it suffers from, like low sensitivity at clinical doses, nonuniformity across the film

The development of electronic portal imaging devices (EPIDs) has made it a popular tool for online verification. Work in this area has been presented by other groups (Louwe *et. al* 2003, Chang *et al.* 2003). This would save much time and make the whole verification procedure less laborious. However, there is still too little experience with EPID as a dosimetric detector in the clinic.

V. ACKNOWLEDGEMENT

The author would like to thank the supervisors Tommy Knöös and Per Nilsson for their excellent guiding through this whole work. The whole semester has been very stimulating. And also thanks to all the other staff at the clinic for taking their time to help with all the problems that popped up, which have been more than I ever expected before this study. And finally but not least, also many thanks to Petra Ambolt for her company through many days and late nights with fruitful discussions.

VI. REFERENCES

1. Adams E.J., Convery D.C., Cosgrove V.P., McNair H.A., Staffurth N., Vaarkamp J., Nutting C.M., Warrington A.P., Webb S., Balyckyi J., Dearnaley D.P, *"Clinical implementation of dynamic and step-and-shoot IMRT to treat prostate cancer with high risk of pelvic lymph node involvement"*, Rad. and Onc. **70,** 2003, 1-10.
2. Ambolt P., *"Intensity Modulated Radiotherapy Treatment Planning with OTP/TMS for Head & Neck Carcinomas in the ARTSCAN study"*, Master of science thesis 2004, Department of Medical Radiation Physics, The Jubileum Institute, Lund University.
3. Amols H.I., Ling C.C., Leibel S.A., *"A practical guide to intensity-modulated radiation therapy*", Overview of the IMRT process, chap. 2, 2003, ISBN 1-930524-13-7.
4. Brahme A., Roos J-E. Lax I., *"Solution of an integral equation encountered in rotation therapy"*, Phys. Med. Biol. **27** (10), 1982, 1221-1229.
5. Bäck A., *"Intensity Modulated Radiation Therapy in the Head and Neck Region using Dynamic Multi-Leaf Collimation"*, Doctorial Thesis, Department of Radiation Physics Gothenburg University 2003, ISBN 91-628-5628-6.
6. Bakai A., Alber M., Nüsslin F., *"A revision of the γ-evaluation concept for the comparison of dose distributions"*, Phys. Med. Biol. **48,** 2003, 3543-3553.
7. Cadman P., Bassalow R., Sidhu N.P., Ibbott G., Nelson A., *"Dosimetric considerations for validation of a sequential IMRT process with a commercial treatment planning system"*, Phys. Med. Biol. **47,** 2002, 3001-3010.
8. Carlson D., *"Intensity modulation using multileaf collimators: current status"*, Med. Dos. **26** (2), 2001, 151-156.
9. Chang J., Mageras G.S., Ling C.C., *"Evaluation of rapid dose map acquisition of a scanning liquid-filled ionization chamber electronic portal imaging device"*, Int. J. Radiat. Oncol. Biol. Phys., 1;55(5), April 2003, 1432-45.
10. Chui C-S., Chan M.F., Yorke E., Spirou S., Ling C., *"Delivery of intensity-modulated radiation therapy with a conventional multileaf collimator: Comparison of dynamic and segmental methods"*, Med. Phys. **28** (12), December 2001, 2441-2449.
11. van Esch A., Bohsung J., Sorvari P., Tenhunen M., Paiusco M., Iori M., Engström P., Nyström H., Huyskens D.P., *"Acceptance tests and quality control (QC) procedures for the clinical implementation of intensity modulated radiotherapy (IMRT) using inverse planning and the sliding window technique: experience from five radiotherapy departments"*, Rad. and Onc. **65,** 2002, 53-70.
12. Esthappan J., Mutic S., Harms W.B., Dempsey J.F., Low D.A., *"Dosimetry of therapeutic photon beams using an extended dose range film"*, Med. Phys. **29** (10), October 2002, 2438-2545.
13. Ezzell G.A., Galvin J.M., Low D., Palta J.R., Rosen I., Sharpe M.B., Xia P., Xiao Y., Xing L., Yu C.X., *"Guidance document on delivery, treatment*

planning, and clinical implementation of IMRT: Report of the IMRT subcommittee of the AAPM radiation therapy committee", Med. Phys. **30** (8), August 2003, 2089-22115.

14. Mijheer B., Olszewska A., Knöös T., Fiorino C., Rosenwald J-C., *"Quality assurance of treatment planning systems – practical examples for non-IMRT photon beams"*, ESTRO Booklet No. 7 (to be published).
15. Harms W.B., Low D.A., Wong J.W., Purdy J.A., *"A software tool for the quantitative evaluation of 3D dose calculation algorithms"*, Med. Phys. **25** (10), October 1998, 1830-1836.
16. ICRU (International Commission on Radiation Units and measurements), *"Use of computers in external beam radiotherapy procedures with high energy photons and electrons"*, ICRU Report 42, 1987.
17. Knöös T., Ceberg C., Weber L., Nilsson P., *"The dosimetric verification of a pencil beam based treatment planning system"*, Phys. Med. Biol. **39,** 1994, 1609-1628.
18. Laub W.U., Wong T., *"The volume effect of detectors in the dosimetry of small fields used in IMRT"*, Med. Phys. **30** (3), March 2003, 341-347.
19. Leybovich L.B., Sethi A., Dogan N., *"Comparison of ionization chambers of various volumes for IMRT absolute dose verification"*, Med. Phys. **30** (2), February 2003, 119-123.
20. LoSasso T., Chui C-S., Ling C.C., *"Comprehensive quality assurance for the delivery of intensity modulated radiotherapy with a multileaf collimator used in the dynamic mode"*, Med. Phys. **28** (11), November 2001, 2209-2219.
21. LoSasso T., *"A practical guide to intensity-modulated radiation therapy*", Quality Assurance Of IMRT, chap. 8, 2003, ISBN 1-930524-13-7.
22. Louwe R.J., Damen E.M., van Herk M., Minken A.W., Torzsok O., Mijnheer B.J., *"Three-dimensional dose reconstruction of breast cancer treatment using portal imaging"*, Med. Phys. **30** (9), September 2003, 2376-2389.
23. Low D.A., Harms W.B., Mutic S., Purdy J.A., *"A technique for the quantitative evaluation of dose distributions"*, Med. Phys. **25** (5), May 1998, 656-661.
24. Olch A.J., *"Dosimetric performance of an enhanced dose range radiographic film for intensity-modulated radiation therapy quality assurance",* Med. Phys. **29** (9), September 2002, 2159-2168.
25. Price R.A., Li J., Yang J., McNeeley S.W., Chen L., Fourkal E., Ding M., Xiong W., Qin L., Mora G., Ma C. C-M., *"IMRT QA Analysis: What to do with unresolved discrepancies"*, ASTRO 2003.
26. SBU-rapport nr 129/1 1996 chap. 3, *"Vad är strålning"*, ISBN 91-87890-32-1.
27. Venselaar J., Welleweerd H., Mijnheer B., *"Tolerances for the accuracy of photon beam dose calculations of treatment planning systems"*, Rad. and Onc. **60,** 2001, 191-201.
28. Xia P., Verhey L. J., *"Delivery systems of intensity-modulated radiotherapy using conventional multileaf collimators"*, Med. Dos., **26** (2), 2001, 169-177.

29. Zhu X.R., Jursinic P.A., Grimm D.F., Lopez F., Rownd J.J., Gillin M.T., *"Evaluation of Kodak EDR2 film for dose verification of intensity modulated radiation therapy delivered by a static multileaf collimator"*, Med. Phys. **29** (8), August 2002, 1687-1692.